



1   **Spatial and temporal variations in snow chemistry along a traverse**  
2   **from coastal East Antarctica to the ice sheet summit (Dome A)**

3  
4   Guitao Shi<sup>1,2</sup>, Hongmei Ma<sup>2</sup>, Zhengyi Hu<sup>2</sup>, Zhenlou Chen<sup>1</sup>, Chunlei An<sup>2</sup>, Su Jiang<sup>2</sup>, Yuansheng Li<sup>2</sup>,  
5   Tianming Ma<sup>2</sup>, Jinhai Yu<sup>2</sup>, Danhe Wang<sup>1</sup>, Siyu Lu<sup>2</sup>, Bo Sun<sup>2</sup>, and Meredith G. Hastings<sup>3</sup>

6   <sup>1</sup> Key Laboratory of Geographic Information Science (Ministry of Education), School of Geographic  
7   Sciences and State Key Lab of Estuarine and Coastal Research, East China Normal University,  
8   Shanghai 200241, China

9   <sup>2</sup> Polar Research Institute of China, Shanghai 200062, China,

10   <sup>3</sup> Department of Earth, Environmental and Planetary Sciences and Institute at Brown for Environment  
11   and Society, Brown University, Providence, Rhode Island 02912, USA.

12   \*Correspondence to: G Shi (gtshi@geo.ecnu.edu.cn)

13



14 **Abstract**

15 There is a large variability in environmental conditions across the Antarctic ice sheet, and it is of  
16 significance to investigate the snow chemistry at as many locations as possible and over time, given  
17 that the ice sheet itself, and precipitation and deposition patterns and trends are changing. The China  
18 inland Antarctic traverse from coastal Zhongshan Station to the ice sheet summit (Dome A) covers a  
19 variety of environments, allowing for a vast collection of snow chemistry conditions across East  
20 Antarctica. Surface snow and snow pit samples were collected on this traverse during five campaigns,  
21 to comprehensively investigate the spatial and temporal variations in chemical ions ( $\text{Cl}^-$ ,  $\text{NO}_3^-$ ,  $\text{SO}_4^{2-}$ ,  
22  $\text{Na}^+$ ,  $\text{NH}_4^+$ ,  $\text{K}^+$ ,  $\text{Mg}^{2+}$ , and  $\text{Ca}^{2+}$ ) and the related controlling factors. Results show that spatial patterns of  
23 ions in surface snow are consistent among the five campaigns, with  $\text{Cl}^-$ ,  $\text{Na}^+$ ,  $\text{K}^+$ , and  $\text{Mg}^{2+}$  decreasing  
24 rapidly with distance from the coast and  $\text{NO}_3^-$  showing an opposite pattern. No clear spatial trends in  
25  $\text{SO}_4^{2-}$ ,  $\text{NH}_4^+$ , and  $\text{Ca}^{2+}$  were found. In the interior areas, an enrichment of  $\text{Cl}^-$  versus  $\text{Na}^+$  with respect to  
26 seawater composition is ubiquitous as a result of the deposition of  $\text{HCl}$ , which can account for up to  
27  $\sim 40\%$  of the total  $\text{Cl}^-$  budget, while enriched  $\text{K}^+$  and  $\text{Mg}^{2+}$  are associated with terrestrial particle mass.  
28  $\text{Ca}^{2+}$  and  $\text{SO}_4^{2-}$  in surface snow are significantly enriched relative to  $\text{Na}^+$ , related to terrestrial dust  
29 inputs and marine biogenic emissions, respectively. Snow  $\text{NH}_4^+$  is mainly associated with marine  
30 biological activities, with higher concentrations in summer than in winter. On the coast, parts of the  
31 winter snow are characterized with a depletion of  $\text{SO}_4^{2-}$  versus  $\text{Na}^+$ , and a significant negative  
32 correlation between  $\text{nssSO}_4^{2-}$  and  $\text{Na}^+$  was found, suggesting that sea salts originated from the sea ice.  
33 In the interior areas, the negative  $\text{nssSO}_4^{2-}$  signal in winter snow resulted from inputs of sea salts being  
34 completely swamped by the contribution of marine biogenic emissions. Ternary plots of  $\text{Cl}^-$ ,  $\text{Na}^+$ , and  
35  $\text{SO}_4^{2-}$  suggest that sea salt modification is generally negligible on the coast, while the degree of  
36 modification processes to sea salts is high in the interior areas, especially during the summertime. Ion  
37 flux assessment suggests an efficient transport of  $\text{nssSO}_4^{2-}$  to at least as far inland as the  $\sim 2800$  m  
38 contour line. The interannual variations in ion concentrations in surface snow on the traverse are likely  
39 linked to the changes in the Southern Indian Ocean low (SIOL) from year to year, and the deepening of  
40 the SIOL in summer tends to promote the transport of marine aerosols to Princess Elizabeth Land.

41  
42



## 43 1 Introduction

44 Snow can scavenge the atmospheric chemicals, including sea salts, acids and other organic species,  
45 and thereby ice cores can provide the most direct records of the composition of the atmosphere. In  
46 Antarctica, the EPICA Dome C ice core encompassed more than 800 ka of sequential glaciochemical  
47 data, the longest available records obtained thus far from ice cores (EPICA Community Members, 2004;  
48 Wolff et al., 2006; Jouzel et al., 2007; Kaufmann et al., 2010). Major chemical ions are among the core  
49 classical measurements in snow and ice due to that they are indicative of a wealth of climate  
50 information (e.g., marine biological activity, sea ice extent, and atmospheric circulation pattern). In  
51 comparison with trace gases trapped in ice core bubbles, the accurate interpretation of glaciochemical  
52 records is challenging since chemicals in the ice can be indicative of a combination of sources,  
53 transport strength, and preservation processes. At times, records of a particular species in ice cores can  
54 be interpreted differently amongst sites, e.g., sodium ( $\text{Na}^+$ ) variability in ice cores might indicate the  
55 changes in sea ice extent or atmospheric meridional transport strength at varied locations (Goodwin et  
56 al., 2004; Severi et al., 2017). Therefore, there has been great interest in the determination of sources,  
57 mechanisms, and pathways of transport as well as preservation mechanisms of chemicals in snow and  
58 ice (e.g., Mahalinganathan et al., 2011; Dixon et al., 2013; Shi et al., 2018a), and a better understanding  
59 of snow chemistry is crucial towards an accurate interpretation of glaciochemical records from ice  
60 cores.

61 Snow chemistry has been broadly investigated along traverses during the International  
62 Trans-Antarctic Scientific Expedition (ITASE), e.g., DDU to Dome C, Syowa to Dome F, Terra Nova  
63 Bay to Dome C, 1990 ITASE, and US ITASE in West Antarctica (Qin et al., 1992; Mulvaney and Wolff,  
64 1994; Proposito et al., 2002; Suzuki et al., 2002; Dixon et al., 2013), and Bertler et al. (2005) has  
65 comprehensively summarized the glaciochemical data across the ice sheet, most of which are for  
66 surface snow. Among the major ions, sea salt related ions (e.g.,  $\text{Na}^+$  and  $\text{Cl}^-$ ), in general, are the most  
67 abundant species, and typically exhibit a clear spatial trend, with concentrations falling off sharply with  
68 distance from the coast. Sea salts in snow are traditionally thought to be from sea spray in open water,  
69 and higher wind speeds (more efficient production and transport) are proposed to be responsible for the  
70 higher sea salt concentrations in winter (Delmas, 1992). Recently, sea salt aerosols produced from  
71 blowing snow above sea ice is thought to be a major source of sea salt related ions (Wolff et al., 2003;  
72 Frey et al., 2020), and this tends to well explain their higher concentrations in the winter snow. Also, it  
73 is proposed that sea salt aerosols originated from sea ice can be efficiently transported to central  
74 Antarctica (Udisti et al., 2012; Legrand et al., 2017b), and thus sea salts can be a proxy in ice cores for  
75 sea ice coverage (Abram et al., 2013 and references therein). Acidic ions such as nitrate and sulfate  
76 ( $\text{NO}_3^-$  and  $\text{SO}_4^{2-}$ ) are typically also abundant ionic species in snow, both of which can be deposited as  
77 salts in aerosols, and as gaseous acids.  $\text{SO}_4^{2-}$  in the snow is mainly from marine biogenic sulfur species,  
78 dimethylsulphide (DMS) (Saltzman, 1995), with a small proportion from sea salt aerosols, while large  
79 volcanic eruption emissions can episodically contribute to spikes in  $\text{SO}_4^{2-}$  concentration (Jiang et al.,  
80 2012; Cole-Dai et al., 2013). Thus,  $\text{SO}_4^{2-}$  in ice cores can be indicative of ocean productivity in the past  
81 (e.g., Wolff et al., 2006). Sources of  $\text{NO}_3^-$  are sometimes complicated to identify, due to the  
82 post-depositional processing after deposition into the snowpack (e.g., photolysis and volatilization),  
83 and stratospheric input and tropospheric transport from mid-low latitudes have been proposed to be  
84 important sources (Wagenbach et al., 1998b; Savarino et al., 2007; Lee et al., 2014; Shi et al., 2015;  
85 Shi et al., 2018a). As for calcium ( $\text{Ca}^{2+}$ ) in snow, both long range transport of terrestrial particle mass  
86 and sea salt aerosols are important sources, and  $\text{Ca}^{2+}$  in ice cores recovered from interior areas is more



87 likely associated with terrestrial inputs (e.g., Wolff et al., 2006). Terrestrial sources can also contribute  
88 to potassium ( $K^+$ ) and magnesium ( $Mg^{2+}$ ) in snow, but the contribution proportion varies significantly  
89 among sites (Keene et al., 2007; Khodzher et al., 2014). In comparison with the other species,  
90 ammonium ( $NH_4^+$ ) in the snow has been rarely investigated due to the low concentration, and biogenic  
91 emissions in the Southern Ocean and/or mid-latitude biomass burning were proposed to be the major  
92 sources, depending on the investigation sites (Kaufmann et al., 2010; Pasteris et al., 2014). In summary,  
93 source identification of ions in Antarctic snow and ice has been conducted intensely, however, the site-  
94 and area-specific investigations are needed.

95 With varied sources and lifetimes, ions in snow often exhibit different seasonal variations, e.g., sea  
96 salt related ions show high concentrations in winter, while elevated concentrations of  $SO_4^{2-}$  and  $NO_3^-$   
97 are frequently observed in summer (e.g., Wagenbach, 1996; Gragnani et al., 1998; Traversi et al., 2004;  
98 Shi et al., 2015). Indeed, these ions are frequently taken as seasonal markers for snow pit and ice core  
99 dating. On annual to decadal time scales, ion concentrations in snow and ice tend to be associated with  
100 changes in transport from year to year (Xiao et al., 2004; Severi et al., 2009), and thus large scale  
101 atmospheric and oceanic circulation in the Southern Hemisphere, such as the Southern Annular Mode  
102 (SAM), Southern Oscillation (SO) and Southern Indian Ocean Dipole (SIOD), could potentially  
103 influence variations in ions in ice (Russell and McGregor, 2010; Mayewski et al., 2017). For instance,  
104 the variability of  $Na^+$  in the Law Dome ice core was mostly like associated with interannual changes in  
105 SAM that dominates the meridional aerosol transport from mid-latitude sources (Goodwin et al., 2004).  
106 In addition, sea ice coverage around Antarctica plays an important role in variations in ions, and larger  
107 sea ice coverage is linked with higher sea salt concentrations, as well as non-sea salt  $SO_4^{2-}$  ( $nssSO_4^{2-}$ )  
108 concentrations in ice, particularly over glacial-interglacial time scales (Kaufmann et al., 2010; Wolff et  
109 al., 2010; Abram et al., 2013). In addition to sources, lifetime, and transport processes, the preservation  
110 of ions is an important factor influencing concentrations in snow and ice, particularly the volatile  
111 species (e.g.,  $NO_3^-$  and  $Cl^-$ ). Post-depositional processes can result in significant losses of volatile  
112 species in snow, particularly at sites with low snow accumulation rate (e.g., East Antarctic plateau)  
113 (Wagnon et al., 1999; Sato et al., 2008; Shi et al., 2015). In summary, spatial and temporal variations in  
114 snow chemistry are influenced by a variety of factors, and further observations of ions in snow are  
115 needed to determine the controlling factors for particular times and places.

116 Although investigations of snow chemistry have been carried out along several overland traverses,  
117 many Antarctic areas remain undocumented. In addition, the Antarctic ice sheet itself, and precipitation  
118 and deposition patterns and trends are changing, and the investigation of snow chemistry under  
119 different environmental conditions and over time is needed. The China inland Antarctic traverse from  
120 coastal Zhongshan Station to the ice sheet summit (Dome A) covers a distance of 1256 km in the  
121 Indian Ocean sector. The first China inland Antarctic expedition took place in 1999, reaching the site  
122 ~300 km from the coast, and in 2005, this traverse extended to Dome A plateau (with elevation ~4100  
123 m), where the oldest ice (~one million-year old) was thought to be preserved (Zhao et al., 2018). This  
124 traverse covers a range of environments, e.g., high snow accumulation rate is present on the coast and  
125 in some interior areas, and very low accumulation rate is observed on the Dome A plateau. It is noted  
126 that some of the interior areas are greatly influenced by persistent wind scour, leading to near zero  
127 snow accumulation (Das et al., 2013; Ding et al., 2015). This traverse, thus, provides further  
128 opportunity to investigate snow chemistry and its main controlling factors in different environments. In  
129 addition, the Dome A deep ice core reached a depth of 803 m in 2019, and an investigation of snow  
130 chemistry in the Indian Ocean sector, especially on the Dome A plateau would be of significance to the



131 interpretation of the deep ice core. Several investigations have been carried out in the past to determine  
132 the concentrations and spatial patterns of a few ionic species and trace elements on the traverse (e.g., Li  
133 et al., 2016; Du et al., 2019), but limited snow chemistry data were previously available. Additionally,  
134 the interannual variations in snow chemistry and the related controlling factors on the traverse are far  
135 from understood. Therefore, we used surface snow and snow pit samples collected during five China  
136 inland Antarctic scientific expedition campaigns, to determine the spatial and temporal variations in a  
137 comprehensive set of ions ( $\text{Na}^+$ ,  $\text{NH}_4^+$ ,  $\text{K}^+$ ,  $\text{Mg}^{2+}$ ,  $\text{Ca}^{2+}$ ,  $\text{Cl}^-$ ,  $\text{NO}_3^-$ , and  $\text{SO}_4^{2-}$ ) and their controlling  
138 factors. This work also presents data on snow chemistry from a less documented area, particularly the  
139 Dome A area, providing baseline values of snow ions and records of significance for evaluating  
140 potential changes in atmospheric chemistry over Antarctica under a warming climate.

141

## 142 **2 Methods**

### 143 **2.1 Sample collection**

144 Snow samples were collected along the traverse from the coast to the ice sheet summit during five  
145 Chinese National Antarctic Research Expedition (CHINARE) campaigns (Fig. 1). In January 1999, 107  
146 surface snow samples were collected on the traverse (from coast to the site ~1100 km from the coast;  
147 the Chinese inland traverse coverage did not extend to Dome A then). In January and February in the  
148 years 2011, 2013, 2015, and 2016, 120, 125, 117, and 125 surface snow samples were collected on the  
149 traverse, respectively. In total, 594 snow samples were collected during the five seasons.

150 Surface snow samples were collected at ~10 km intervals, and the sampling sites are generally >500  
151 m away from the traverse route to avoid possible contamination from expedition team activities.  
152 During snow sampling, all personnel wore polyethylene (PE) gloves and face masks, and pushed the  
153 high-density polyethylene (HDPE) bottles horizontally into the surface snow layer (~3 cm) in the  
154 windward direction.

155 In addition to surface snow, snow pits were sampled in three representative areas on the traverse (P1,  
156 P2, and P3; Fig. 1). P1, located on the coast (76.49 °E, 69.79 °S; 46 km from the coast), was sampled in  
157 December 2015; P2, located in the interior area (77.03 °E, 76.42 °S; 800 km from the coast), was  
158 sampled in January 2016; P3, located on Dome A plateau (77.11 °E, 80.42 °S; 1256 km from the coast),  
159 was sampled in January 2010. Sites P1 and P2 are characterized with high snow accumulation rate  
160 (>100 kg m<sup>-2</sup> a<sup>-1</sup>), while snow accumulation rate at P3 is ~25 kg m<sup>-2</sup> a<sup>-1</sup>. The depths of P1, P2, and P3  
161 are 180, 100, and 150 cm, respectively, with the respective sampling resolution of 5, 3, and 1 cm. Snow  
162 pit samples were collected using the narrow mouth HDPE bottles pushed horizontally into the snow  
163 wall from the bottom of the pit and moving upwards.

164 All of the bottles used for snow sampling were pre-cleaned with Milli-Q water (18.2 MΩ), dried in a  
165 class 100 super clean hood and then sealed in clean PE bags that were not opened until the field  
166 sampling started. During each sampling campaign, three pre-cleaned bottles filled with Milli-Q water  
167 taken to the field and treated to the same conditions as field samples represent field blanks. After  
168 collection, the bottles were again sealed in clean PE bags and preserved in clean expanded  
169 polypropylene boxes. All samples were transported and stored under freezing conditions (~-20 °C).

170

### 171 **2.2 Sample analysis**

172 Snow samples were first melted in the closed bottles on a super clean bench (class 100) before  
173 chemical measurements. In the class 100 room, about 5 ml of the melted sample was transferred to the  
174 pre-cleaned 8-ml ion chromatography (IC) autosampler vials, and then the lid was tightly screwed on to



175 the vials. The samples were analyzed by IC for the concentrations of ions ( $\text{Na}^+$ ,  $\text{NH}_4^+$ ,  $\text{K}^+$ ,  $\text{Mg}^{2+}$ ,  $\text{Ca}^{2+}$ ,  
176  $\text{Cl}^-$ ,  $\text{NO}_3^-$ , and  $\text{SO}_4^{2-}$ ). (Note that the IC was installed in a class 1000 clean room) The samples collected  
177 in 1999 were analyzed by using the DX-500 IC system (Dionex, USA), while the snow collected in the  
178 other campaigns were analyzed using an ICS-3000 IC system (Dionex, USA). The eluents for cations  
179 and anions were methanesulfonic acid (MSA) and potassium hydroxide (KOH), respectively. More  
180 details on this method are described in Shi et al. (2012). During sample analysis, replicate  
181 determinations ( $n = 5$ ) were performed, and one relative standard deviation ( $1\sigma$ ) for all eight ions was  
182 generally  $<5\%$ . In addition, the pooled standard deviation of all replicate samples run in at least two  
183 different sets was examined ( $n = 65$ ) and yielded 0.020, 0.023, 0.038, 0.022, 0.039, 0.005, 0.008, and  
184  $0.005 \mu\text{eq L}^{-1}$  for  $\text{Cl}^-$ ,  $\text{NO}_3^-$ ,  $\text{SO}_4^{2-}$ ,  $\text{Na}^+$ ,  $\text{NH}_4^+$ ,  $\text{K}^+$ ,  $\text{Mg}^{2+}$ , and  $\text{Ca}^{2+}$ , respectively. Ion concentrations in  
185 field blanks are lower than the detection limit (DL, 3 standard deviations of water blank in the  
186 laboratory).

187 In Antarctic snow, concentrations of  $\text{H}^+$  are usually not measured directly, but deduced from the  
188 ion-balance disequilibrium in the snow. Here,  $\text{H}^+$  concentration is calculated as follows.

$$189 [\text{H}^+] = [\text{SO}_4^{2-}] + [\text{NO}_3^-] + [\text{Cl}^-] - [\text{Na}^+] - [\text{NH}_4^+] - [\text{K}^+] - [\text{Mg}^{2+}] - [\text{Ca}^{2+}] \text{ Eq. (1)}$$

190 where ion concentrations are in  $\mu\text{eq L}^{-1}$ . In addition, the non-sea-salt fractions of ions (nssX), including  
191 nssCl<sup>-</sup>, nssSO<sub>4</sub><sup>2-</sup>, nssK<sup>+</sup>, nssMg<sup>2+</sup> and nssCa<sup>2+</sup>, can be calculated from the following expression,

$$192 [\text{nssX}] = [\text{X}]_{\text{snow}} - ([\text{X}]/[\text{Na}^+]_{\text{seawater}} \times [\text{Na}^+]_{\text{snow}} \text{ Eq. (2)}$$

193 where [X] is the concentration of ion X, and [X]/[Na<sup>+</sup>] ratios in seawater are 1.17 (Cl<sup>-</sup>), 0.12 (SO<sub>4</sub><sup>2-</sup>),  
194 0.022 (K<sup>+</sup>), 0.23 (Mg<sup>2+</sup>) and 0.044 (Ca<sup>2+</sup>) (in  $\mu\text{eq L}^{-1}$ ).

195

### 196 2.3 Enrichment assessment of ions

197 The enrichment factor (EF) is a measurement of whether or not an ion is present in a relative  
198 abundance similar to that of seawater, which can be calculated as follows.

$$199 \text{EF}_X = ([\text{X}]/[\text{Na}^+]_{\text{snow}}) / ([\text{X}]/[\text{Na}^+]_{\text{seawater}} \text{ Eq. (3)}$$

200 When  $\text{EF} > 1.0$ , the ion X is enriched, i.e., additional sources are present in addition to sea salt spray.  
201  $\text{EF} < 1.0$  corresponds to the depletion of ion X, possibly indicating the presence of fractionation.

202 In both equations (2) and (3), we assume that  $\text{Na}^+$  is exclusively from the sea spray (i.e., the sea salt  
203 indicator) in surface snow based on the following facts: 1) the Cl/Na<sup>+</sup> ratios in snow samples are  
204 generally above 1.17, the average value in seawater (Nozaki, 2001), 2) the contribution of dust  
205 leachable Na is negligible in Antarctic snow (Legrand and Delmas, 1988; Röthlisberger et al., 2002),  
206 and 3) negligible Na<sup>+</sup> fractionation resulted from mirabilite ( $\text{Na}_2\text{SO}_4 \cdot 10\text{H}_2\text{O}$ ) precipitation in sea-ice  
207 formation at  $<-8^\circ\text{C}$  (Marion et al., 1999), especially considering the smallest sea ice extent in late  
208 summer in East Antarctica (Holland et al., 2014).

209

### 210 2.4 Principal component analysis (PCA) of ions

211 The essence of PCA is converting the observed variables into factors or principal components, so  
212 that a minimized set of underlying variables can be identified. Bartlett sphericity test and  
213 Kaiser-Meyer-Olkin test indicated that the raw data (i.e., ion concentrations in surface snow) were  
214 suitable for PCA ( $p < 0.001$ ). Varimax with Kaiser normalization rotation was applied to maximize the  
215 variances of the factor loadings across variances for each factor. The regression method was selected  
216 for calculating the factor score coefficient. Three components with eigenvalue  $> 1.0$  were extracted. The  
217 loadings were obtained from the eigenvalues of the three components and their corresponding  
218 eigenvectors.



219 Because the samples collected in 1999 did not cover the whole traverse and the ion concentrations  
220 were determined using a different IC system, the ion data of 1999 were excluded in the EF and PCA  
221 analysis in the following.

222

### 223 3 Results

#### 224 3.1 Ion concentrations in surface snow

225 Concentrations of ions in surface snow collected during the five seasons are shown in Fig. 2, and the  
226 ranges (mean) of  $\text{Cl}^-$ ,  $\text{NO}_3^-$ ,  $\text{SO}_4^{2-}$ ,  $\text{Na}^+$ ,  $\text{NH}_4^+$ ,  $\text{K}^+$ ,  $\text{Mg}^{2+}$  and  $\text{Ca}^{2+}$  are 0.15-14.6 (1.29), 0.48-12.6 (3.37),  
227 0.37-5.63 (1.52), 0.09-12.74 (0.68), 0.04-0.77 (0.16), 0.01-0.27 (0.04), 0.11-2.76 (0.22) and 0.01-0.50  
228 ( $0.13 \mu\text{eq L}^{-1}$ ), respectively. These values fall within the reported ranges of the ITASE program  
229 sampling (Bertler et al., 2005). Ion concentrations are both spatially and temporally variable, with the  
230 coefficient of variation (ratio of one standard deviation over mean) of  $>0.48$ , suggesting a large  
231 variability across the traverse. In general, ion concentrations do not follow a normal distribution  
232 ( $p > 0.05$ , One-Sample Kolmogorov-Smirnov Test), with the values of skewness and kurtosis above 1.0,  
233 but they correspond to a logarithmic normal distribution.

234 pH values of surface snow sampled in 2013 were measured with a glass pH electrode, and  $\text{H}^+$   
235 concentrations deduced from pH are correlated well with the values calculated from the ion-balance  
236 method (Fig. 3(a)). On average,  $\text{H}^+$  concentrations obtained from the ion balance approach are  $\sim 25\%$   
237 lower than those deduced from pH. It is noted that pH measurements in this study remain uncertain  
238 considering that snow samples are highly undersaturated with respect to carbon dioxide ( $\text{CO}_2$ )  
239 immediately after melting in the lab (Pasteris et al., 2012). On the other hand, organic acids, e.g.,  
240 monocarboxylic and methanesulfonic acids (MSA), were excluded in  $\text{H}^+$  calculation (Eq. 1), although  
241 their concentrations in Antarctic snow tend to be very low (Li et al., 2015; Li et al., 2016). If the  
242 contribution of organic acids to  $\text{H}^+$  in the snow is negligible, the x-intercept of  $\sim 2.4 \mu\text{eq L}^{-1}$  in the linear  
243 regression (Fig. 3(a)) can be regarded as the contribution from dissolved  $\text{CO}_2$  in snow during pH  
244 measurements. This value is close to that of pure water in equilibrium with  $\text{CO}_2$  in the atmosphere,  
245 with  $\text{pH}=5.6$  corresponding to  $\text{H}^+$  concentration of  $\sim 2.5 \mu\text{eq L}^{-1}$ .

246 The percentage of each constituent to the total ions in surface snow is shown in Fig. 3(b). The most  
247 abundant species is  $\text{H}^+$ , accounting for 39.6 % of the total ions, followed by  $\text{NO}_3^-$  and  $\text{SO}_4^{2-}$ ,  
248 representing 27.5 and 12.5 % of the total ion budget, respectively. The high contribution percentage of  
249  $\text{H}^+$  is consistent with previous investigations (Udisti et al., 2004; Traversi et al., 2009; Pasteris et al.,  
250 2014), suggesting the acidic characteristics of surface snow. In general, ions  $\text{NH}_4^+$ ,  $\text{K}^+$ ,  $\text{Mg}^{2+}$ , and  $\text{Ca}^{2+}$   
251 are the smallest component of the ionic composition, with the four cation summing to  $\sim 5\%$  of the total.

252 Previous investigations of ions in surface snow covered various depths among different traverses or  
253 campaigns, e.g., 1.0 m deep layer for the traverse from Terra Nova Bay to Dome C and top 25 cm snow  
254 for the 1990 ITASE (Qin et al., 1992; Proposito et al., 2002). It is noted that different sampling depths  
255 can result in varied ion concentrations in snow. For instance, in inland Antarctica,  $\text{NO}_3^-$  is often  
256 concentrated on the top few-centimeter snow, and decreases significantly with increasing depth (Shi et  
257 al., 2015). Thus, any comparison of ion concentrations in surface snowpack collected from different  
258 campaigns should be made with caution.

259

#### 260 3.2 Spatial patterns of ions in surface snow

261 The spatial distribution patterns of ions on the traverse are consistent among the five campaigns (Fig.  
262 2). In general,  $\text{Cl}^-$ ,  $\text{Na}^+$ ,  $\text{K}^+$ , and  $\text{Mg}^{2+}$  show very high concentrations within the narrow coastal region,



263 and decrease sharply further inland, with low values on Dome A plateau (~1000-1250 km from the  
264 coast). It is noted that some samples on the coast also show elevated  $\text{Ca}^{2+}$  concentrations. The spatial  
265 patterns are consistent with previous observations (Bertler et al., 2005; Kärkäs et al., 2005), and the  
266 high ion concentrations near the coast have been explained by the strong marine air mass intrusions  
267 (Hara et al., 2014).

268 Different from other species,  $\text{NO}_3^-$  concentrations near the coast are low, and increase towards inland,  
269 with the highest values on the Dome A plateau. A significant correlation is found between  $\text{NO}_3^-$  and  
270 distance from the coast, with  $r = 0.56$  and  $p < 0.001$ . The spatial trend of  $\text{NO}_3^-$  is generally opposite to  
271 that of snow accumulation rate on the traverse (Figs. 2(a) and (c)), possibly associated with  
272 post-depositional cycling of  $\text{NO}_3^-$  in surface snow (Erbland et al., 2013; Shi et al., 2018b). Similarly,  
273 there is a close relationship between  $\text{H}^+$  and distance from the coast ( $r = 0.48$ ,  $p < 0.001$ ), suggesting a  
274 higher acidity of inland snow. As for  $\text{SO}_4^{2-}$ ,  $\text{NH}_4^+$ , and  $\text{Ca}^{2+}$ , no clear spatial trend was found on the  
275 traverse.

276

### 277 3.3 Ions in snow pits

278 Clear seasonal cycles of  $\text{Na}^+$  and  $\text{nssSO}_4^{2-}$  are present in P1 and P2, and thus the two pits can be well  
279 dated, spanning ~3 years (Figs. 4(a) and (b)). Based on the snow pit dating, it is estimated that snow  
280 accumulation rate is ~50 (P1) and ~33 cm snow per year (P2), agreeing well with the field  
281 measurements (P1: ~150  $\text{kg m}^{-2} \text{a}^{-1}$ ; P2: ~100  $\text{kg m}^{-2} \text{a}^{-1}$ ; Fig. 2(a)), assuming a snow density of ~0.33  $\text{g}$   
282  $\text{cm}^{-3}$ . At P1, negative  $\text{nssSO}_4^{2-}$  values are observed in winter snow, i.e.,  $\text{SO}_4^{2-}/\text{Na}^+$  ratio below that of  
283 bulk seawater, while all of the  $\text{nssSO}_4^{2-}$  data in P2 pit are positive. It is difficult to assign the samples in  
284 the snow pits to the four distinct seasons based on the measured parameters, and thus, in the following  
285 discussion, we choose a conservative assignment method, i.e., a summer season featured with higher  
286  $\text{nssSO}_4^{2-}$  and  $\text{SO}_4^{2-}/\text{Na}^+$  ratio (and lower  $\text{Na}^+$ ) and a winter season characterized with the opposite  
287 patterns.

288 As for  $\text{nssSO}_4^{2-}$  at P3, the very large signal at the depth of ~120 cm is most likely the fallout from the  
289 massive eruption of Pinatubo in 1991 (Fig. 4(c)), based upon previous observations at Dome A (e.g.,  
290 Hou et al., 2007). Accordingly, the snow accumulation rate from 1992 to 2010 is ~22  $\text{kg m}^{-2} \text{a}^{-1}$ , in line  
291 with previous investigations (Hou et al., 2007; Jiang et al., 2012; Ding et al., 2016). Based on  $\text{nssSO}_4^{2-}$   
292 signals and the method proposed by Cole-Dai et al. (1997), 19 continuous samples have been identified  
293 as influenced by Pinatubo eruption, covering ~2.5 years, possibly suggesting that the effects of  
294 Pinatubo eruption on atmospheric chemistry lasted at least for 2.5 years over Dome A. Interestingly,  
295 only elevated  $\text{SO}_4^{2-}$  concentrations are present during this period, and anomalous high or low  
296 concentrations of other ions are absent. Additionally, no correlation was found between  $\text{nssSO}_4^{2-}$  and  
297 other species during the 2.5 years, suggesting that Pinatubo volcanic emissions contribute less to the  
298 ion budgets other than  $\text{SO}_4^{2-}$  at Dome A.

299 Previous investigations proposed that  $\text{Na}^+$  and  $\text{nssSO}_4^{2-}$  in surface snow (top ~1 cm) collected during  
300 a full year at central Antarctica show clear seasonal cycles, with high (low)  $\text{Na}^+$  in winter (summer)  
301 snow (Udisti et al., 2012). At P3,  $\text{Na}^+$ ,  $\text{nssSO}_4^{2-}$  and the ratios of  $\text{SO}_4^{2-}/\text{Na}^+$  fluctuate significantly, and  
302 these contrasts are unlikely indicative of the seasonal cycles as that for P1 and P2. In a full year of  
303 snow accumulation at P3, on average, 7-8 samples were collected, allowing for examining the seasonal  
304 variability of ions. Following the field measurements of snow accumulation rate at Dome A during  
305 2008-2011 (~20  $\text{kg m}^{-2} \text{a}^{-1}$ ; Ding et al., 2015), the snow samples covering the years 2008 and 2009 can  
306 be roughly identified, assuming an even distribution of snow accumulation throughout the year. In total,



307 there are 7 and 8 samples identified in the years 2008 and 2009, respectively (Fig. 5), and no seasonal  
308 cycles in  $\text{Na}^+$ ,  $\text{nssSO}_4^{2-}$ , and  $\text{SO}_4^{2-}/\text{Na}^+$  ratio were found, maybe related to the post-depositional  
309 processes (e.g., migration, diffusion, and ventilation processes) and/or wind scouring that could  
310 obscure the original signal (Cunningham and Waddington, 1993; Albert and Shultz, 2002; Libois et al.,  
311 2014; Caiazza et al., 2016).

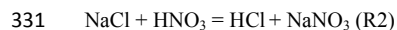
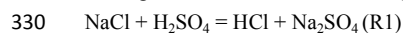
312

#### 313 4. Discussions

##### 314 4.1 Enrichment of ions in surface snow

315 Statistics of enrichment factors (EFs) of ions in surface snow are shown in Fig. 6, and EFs ranges  
316 (means) of  $\text{Cl}^-$ ,  $\text{SO}_4^{2-}$ ,  $\text{K}^+$ ,  $\text{Mg}^{2+}$ , and  $\text{Ca}^{2+}$  are 0.5-6.6 (1.8), 1.5- 87.8 (25.7), 0.7-11.4 (4.6), 0.9-6.2 (2.0),  
317 and 0.2-63.2 (7.3), respectively. Most EFs of  $\text{Cl}^-$ ,  $\text{K}^+$ , and  $\text{Mg}^{2+}$  are close to 1.0, suggesting the main  
318 source of sea salt spray, while most EFs of  $\text{SO}_4^{2-}$  and  $\text{Ca}^{2+}$  are well above 1.0, i.e., greatly enriched,  
319 indicating additional sources. Spatially, EFs of  $\text{Cl}^-$ ,  $\text{K}^+$ ,  $\text{Mg}^{2+}$ , and  $\text{Ca}^{2+}$  at the sites close to the coast are  
320 around 1.0, with elevated values in interior areas, especially on the Dome A plateau.

321 Correlation plots of ions versus  $\text{Na}^+$  in surface snow are shown in Fig. 7, and the plots above (below)  
322 the seawater dilution line represent the enrichment (depletion) of the ions. The further the plots deviate  
323 away from the line, the higher degree of enrichment or depletion of the ions. On the coast, most of the  
324  $\text{Cl}^-/\text{Na}^+$  data are distributed close to the seawater dilution line (Fig. 7(a)), indicating a quantitative sea  
325 salt tracer of snow  $\text{Cl}^-$ , while most of the plots in the interior areas are above the seawater line,  
326 suggesting an enrichment of snow  $\text{Cl}^-$ . On this traverse,  $\text{nssCl}^-$  accounted for an average of 38 % of  
327 total  $\text{Cl}^-$ , with lower (higher) percentages on the coast (plateau), generally in line with previous reports  
328 (e.g., Suzuki et al., 2002). The modifications in  $\text{Cl}^-$  with respect to bulk seawater can occur via the  
329 heterogeneous reactions, as follows (Finlayson-Pitts, 2003),



332 In the atmosphere, the production of HCl will result in depletion of  $\text{Cl}^-$  in sea salt aerosol. The  
333 'secondary' HCl, in the gas phase and/or fine aerosol mode, can be transported further inland due to the  
334 longer lifetime (versus the coarse sea salt aerosols removed preferentially from the atmosphere). In this  
335 case, an enrichment of  $\text{Cl}^-$  would be expected in the inland snowpack. On the other hand,  $\text{Cl}^-$  is not  
336 irreversibly deposited to the snow, and it can be released back into the atmosphere through the  
337 formation of HCl, resulting in an enrichment of  $\text{Cl}^-$  in surface snow via re-deposition. Post-depositional  
338 losses of HCl are thought to be associated with snow accumulation rate, with larger losses occurring at  
339 sites with snow accumulation generally  $<40 \text{ kg m}^{-2} \text{ a}^{-1}$  (Röthlisberger et al., 2003). Indeed, a negative  
340 correlation was found between snow accumulation and  $\text{nssCl}^-$  (Fig. 8(a)) for most interior areas that  
341 featured low snow accumulation and consequently an enhanced cycling of  $\text{Cl}^-$ .

342 Different from  $\text{Cl}^-$ ,  $\text{Mg}^{2+}$  is irreversibly deposited into the snow. Most of the  $\text{Mg}^{2+}/\text{Na}^+$  data points  
343 are above or close to the seawater dilution line, similar to that of  $\text{Cl}^-/\text{Na}^+$  (Fig. 7(d)). On the coast,  
344  $\text{Mg}^{2+}/\text{Na}^+$  data points are in general close to the seawater dilution line, suggesting the main source is  
345 sea salt aerosols, while most of the inland samples are slightly enriched with  $\text{Mg}^{2+}$ , agreeing with  
346 previous observations (e.g., Dome F; Hara et al., 2014). The fraction of  $\text{nssMg}^{2+}$ , on average,  
347 represents  $\sim 36\%$  of  $\text{Mg}^{2+}$  in snow, with lower (higher) values on the coast (plateau). The enrichment of  
348  $\text{Mg}^{2+}$  has not been observed in sea salt particles produced by bubble bursting (Keene et al., 2007), and  
349 thus enriched  $\text{Mg}^{2+}$  in the snow is unlikely associated with sea salt spray. In the atmosphere, sea salt  
350 aerosols would also be modified at low temperatures via the formation of mirabilite (R1), thus leading



351 to an elevated ratio of  $\text{Mg}^{2+}/\text{Na}^+$  if mirabilite precipitate from the aerosols. However, the solid-liquid  
352 separation of mirabilite in the aerosol droplet was not observed in the experiments (Wagenbach et al.,  
353 1998a). Thus, the enrichment of  $\text{Mg}^{2+}$  in surface snow is unlikely associated with sea salt fractionation.  
354 Although it is proposed that  $\text{Mg}^{2+}$  separation in sea salts can occur in surface snow due to the  
355 re-freezing process on surface snow (i.e., the quasi-liquid layers on the crystal surface can act like  
356 seawater freezing; Hara et al., 2014), our measurement of  $\text{Mg}^{2+}$  in bulk snow is unlikely to support this  
357 process responsible for  $\text{Mg}^{2+}$  enrichment. A previous observation conducted near this traverse showed  
358 a moderate correlation of  $\text{Mg}^{2+}$  with element Al in the surface snowpack ( $r=0.53$ ,  $p<0.05$ ), indicating a  
359 contribution of continental dust (Khodzher et al., 2014). Thus, the most plausible interpretation of  
360 enriched  $\text{Mg}^{2+}$  in surface snow is the contribution of terrestrial aerosols.

361 Similar to  $\text{Mg}^{2+}$ , most of  $\text{K}^+/\text{Na}^+$  data points are close to the seawater dilution line on the coast,  
362 suggesting a primary contribution of sea salt spray (Fig. 7(c)). Slightly enriched  $\text{K}^+$  was present in  
363 inland snow, possibly indicating other sources such as biological activity on the coast, mineral  
364 transport, and combustion emissions in Southern Hemisphere (Rankin and Wolff, 2000; Virkkula et al.,  
365 2006; Hara et al., 2013). Given that the sampling sites are at least several tens of kilometers away from  
366 the coast, the contribution of biological activity to snow  $\text{K}^+$  would be rather minor (Rankin and Wolff,  
367 2000). A previous investigation of the atmospheric particles suggests a contribution of combustion in  
368 South America and Southern Africa to atmospheric  $\text{K}^+$  in Antarctica (Hara et al., 2013). Indeed, aerosol  
369 particles from biomass burning in the Southern Hemisphere can be transported to Antarctica, resulting  
370 in the ubiquitous distribution of biomass burning tracers observed in the snow on this traverse (Shi et  
371 al., 2019). However, the average ratio of  $\text{nssK}^+/\text{nssCa}^{2+}$  ( $\sim 0.29$ ) on the traverse is slightly higher than  
372 that of the average crust (0.26; Bowen, 1979), likely supporting a minor contribution of biomass  
373 burning emissions. If  $\text{nssK}^+$  in surface snow is exclusively from terrestrial minerals and combustion  
374 processes, it is estimated that  $\sim 10\%$  of  $\text{nssK}^+$  is originated from biomass burning emissions.

375  $\text{Ca}^{2+}$  is generally enriched versus  $\text{Na}^+$ , with most of the  $\text{Ca}^{2+}/\text{Na}^+$  data points above the seawater  
376 dilution line, especially at inland sites (Fig. 7(e)). The fraction of  $\text{nssCa}^{2+}$ , on average, accounts for  
377  $\sim 77\%$  of total  $\text{Ca}^{2+}$  in surface snow, indicating other dominant sources. In Antarctica, snow  $\text{nssCa}^{2+}$   
378 has been thought to be mainly associated with terrestrial inputs (Bertler et al., 2005; Wolff et al., 2010).  
379 Previous modeling studies suggest that the dust mass reaching East Antarctica mainly originates from  
380 South America, specifically Patagonia (Basile et al., 1997; Wolff et al., 2006; Mahalinganathan and  
381 Thamban, 2016). Metal isotopes in snow collected on this traverse suggested that Australian mineral  
382 dust also can contribute to snow particles (Du et al., 2018). In addition, Antarctic ice free areas were  
383 thought to be a contribution to snow dust (Delmonte et al., 2013; Du et al., 2018). If the dust mass  
384 originated from ice free area near the coast and dominated  $\text{nssCa}^{2+}$ , then  $\text{nssCa}^{2+}$  concentrations near  
385 the coast would be expected to be higher, while the data shows the opposite. Thus, terrestrial dust mass,  
386 possibly from both South America and Australia likely dominates snow  $\text{nssCa}^{2+}$ .

387  $\text{SO}_4^{2-}$  is greatly enriched in all surface snow (Fig. 7(b)), together with the minimum sea ice coverage  
388 around East Antarctica in late summer (Holland et al., 2014), suggesting that sea salts in surface snow  
389 are from open seawater rather than from the sea ice. On the traverse,  $\text{nssSO}_4^{2-}$  represents 33-99 %  
390 (mean=95 %) of total  $\text{SO}_4^{2-}$  in surface snow, with lower (higher) proportions on the coast (plateau). In  
391 Antarctica,  $\text{nssSO}_4^{2-}$  essentially originates from marine biogenic production of DMS (Saltzman, 1995)  
392 and occasionally from explosive volcanism (Cole-Dai et al., 2000; Cole-Dai et al., 2013). In this study,  
393 the significant enrichment of  $\text{SO}_4^{2-}$  suggests a dominant role of ocean bioactivities. Different from the  
394 coarse sea salt aerosols,  $\text{nssSO}_4^{2-}$  can form fine aerosol particles in the atmosphere (Legrand et al.,



2017a), resulting in long atmospheric residence time (>10 days to weeks) and consequently efficient transport (Bondietti and Papastefanou, 1993; Hara et al., 2014). This can help explain the elevated deposition flux of  $\text{nssSO}_4^{2-}$  frequently found at inland Antarctic sites, e.g., site P2 (discussed below). On this transect, a negative relationship was found between snow accumulation rate and  $\text{SO}_4^{2-}$  (or  $\text{nssSO}_4^{2-}$ ) (Figs. 8(c) and (d)), suggesting that snow accumulation rate can influence snow  $\text{SO}_4^{2-}$  concentration, possibly via dilution effects, but overall <~10 % of the variation in  $\text{SO}_4^{2-}$  concentrations can be explained by the relationship.

The ternary diagram of  $\text{Cl}^-$ ,  $\text{Na}^+$ , and  $\text{SO}_4^{2-}$  can well characterize the modification processes to sea salt aerosols, and the ternary plot of the three ions in surface snow is shown in Fig. 9. The values of the ions were normalized via the following equation,

$$X = [X] / ([\text{Na}^+] + [\text{Cl}^-] + [\text{SO}_4^{2-}]) \text{ Eq. (4)}$$

where  $[X]$  is the concentration of ion  $X$  in the snow (in  $\mu\text{eq L}^{-1}$ ). The dashed line between the seawater reference value and the  $\text{SO}_4^{2-}$  vertex represents the sea salt aerosol composition with additional  $\text{SO}_4^{2-}$ , i.e., the ratio of  $\text{Cl}^-/\text{Na}^+$  keeps constant (1.17) with additional  $\text{SO}_4^{2-}$  along the dashed line. The presence of acids ( $\text{HNO}_3$  and  $\text{H}_2\text{SO}_4$ ) would result in the liberation of  $\text{HCl}$  into the atmosphere via reactions R1 and R2, resulting in the changes in  $\text{Cl}^-/\text{Na}^+$  ratios, i.e., either  $\text{Cl}^-$  loss or gain are located right or left of the line, respectively. It is shown that all of the data points are above the seawater plot, suggesting an enrichment of  $\text{SO}_4^{2-}$  in surface snow. Most of the data points are located left of the line, indicating the general enrichment of  $\text{Cl}^-$  due to reactions R1 and R2 occurring in the atmosphere and/or in the snowpack. But the coastal data points are generally close to the line, suggesting that the degree of sea salt modification is generally low in the snow.

416

#### 4.2 Groups of ions in surface snow

PCA is a powerful tool for identifying the common sources and/or transport process of chemicals in different environments. The PCA results (i.e., loadings in each PC), communalities, initial eigenvalues, and explained cumulative percent of the ions in surface snow are listed in Table 1. The first three PCs accounted for 76 % of the variation of the eight original variables. PC1 accounts for 46 % of the variance and is highly loaded by  $\text{Cl}^-$ ,  $\text{Na}^+$ ,  $\text{K}^+$ , and  $\text{Mg}^{2+}$ , with the factor loadings higher than 0.7. In addition, the four species are correlated well with each other (Table 2), suggesting the variation of the four species is dominated by sea salt aerosols, consistent with the EFs results. Thus, PC1 is indicative of the origin of sea salt aerosols.

PC2 accounts for 17 % of the total variance, and the loading values of  $\text{NH}_4^+$  and  $\text{Ca}^{2+}$  in PC2 are high, ~0.8. In Antarctic snow,  $\text{NH}_4^+$  is thought to be mainly associated with biological decomposition of organic matter in the Southern Ocean (Johnson et al., 2007; Kaufmann et al., 2010). In addition, biomass burning from mid-latitudes can contribute to snow  $\text{NH}_4^+$  in West Antarctica (Pasteris et al., 2014). On this transect, no correlation was found between  $\text{NH}_4^+$  and biomass burning tracers on the traverse (Shi et al., 2019), suggesting a minor role of biomass burning emissions. Thus,  $\text{NH}_4^+$  in surface snow tends to be dominated by marine biological activities, and elevated  $\text{NH}_4^+$  concentrations in summer snow would be expected, e.g., summer mean of  $0.23 \mu\text{eq L}^{-1}$  versus winter mean of  $0.16 \mu\text{eq L}^{-1}$  at P1 (Fig. S1). It is proposed that the transport of  $\text{NH}_4^+$  via free troposphere is an important pathway (Kaufmann et al., 2010). Similarly, the meridional transport of particle mass from continents to Antarctica is more efficient in the mid-troposphere (Krinner and Genthon, 2003; Krinner et al., 2010; Shi et al., 2019). Thus, the shared transport process may explain, at least in part, the positive loadings of  $\text{NH}_4^+$  and  $\text{Ca}^{2+}$  in PC2.



439  $\text{NO}_3^-$  is highly loaded in PC3, which accounts for 13 % of the system variance. On this traverse,  $\text{NO}_3^-$   
440 in the snow has been extensively investigated, and it is proposed that  $\text{NO}_3^-$  concentrations were  
441 influenced by post-depositional processing which is largely dependent on snow accumulation rate (Shi  
442 et al., 2015; Shi et al., 2018a; Shi et al., 2018b). A negative relationship was found between  $\text{NO}_3^-$  and  
443 snow accumulation rate (Fig. 8(b)), suggesting a high degree of  $\text{NO}_3^-$  cycling driven by photolysis at  
444 low snow accumulation sites.

445  $\text{SO}_4^{2-}$  did not show high loadings in any of the three extracted components. Its positive loading in  
446 PC1 (0.55) and weak relationships between  $\text{SO}_4^{2-}$  and sea salts ( $\text{Cl}^-$  and  $\text{Na}^+$ ) likely supports the  
447 contribution of sea salt aerosols, although a minor one. A positive loading of  $\text{SO}_4^{2-}$  is also present in  
448 PC3 (0.42), and a weak correlation was found between  $\text{SO}_4^{2-}$  and  $\text{NO}_3^-$ . In summer, snow  $\text{NO}_3^-$  is  
449 mainly produced locally considering that the long-range transported nitrogen compounds can  
450 decompose and undergo rapid  $\text{NO}_x$  cycling in the local boundary layer, and  $\text{NO}_3^-$  production is closely  
451 related to the atmospheric oxidants (Davis et al., 2004; Jones et al., 2011; Morin et al., 2011; Björkman  
452 et al., 2014). Although the main production pathways of  $\text{NO}_3^-$  and  $\text{SO}_4^{2-}$  are different from each other  
453 (Ishino et al., 2017), their formations are closely related to certain oxidant abundances in the  
454 atmosphere (e.g., OH radical), which may partly account for the positive loading of  $\text{SO}_4^{2-}$  in PC3.

455

#### 456 4.3 Ion fluxes and enrichment in snow pits

457 In this section, we discuss the fluxes and enrichment of ions at different depths (i.e., summer and  
458 winter snow) in the three snow pits. The bottom ~30 cm layer of P3 will be excluded in the discussion,  
459 since it represents a snow layer clearly impacted by volcanic (Pinatubo) eruption emissions.

460 Ion fluxes in snow can be determined by multiplying the concentrations by snow accumulation rate,  
461 and the results in the 3 snow pits are shown in Fig. 10. The highest fluxes of ions except for  $\text{NO}_3^-$  were  
462 present at P1, followed by P2 and P3. The flux of  $\text{NO}_3^-$  shows a different pattern, with the highest value  
463 at P2, possibly due to the redistribution of  $\text{NO}_3^-$  across the Antarctic ice sheet driven by photolysis (Shi  
464 et al., 2018b). It is noted that  $\text{nssSO}_4^{2-}$  fluxes at P1 ( $99.4 \pm 46.7 \mu\text{eq m}^{-2} \text{a}^{-1}$ ) and P2 ( $109.2 \pm 21.6 \mu\text{eq m}^{-2}$   
465  $\text{a}^{-1}$ ) are comparable, although P1 is located on the coast and P2 located further inland (~800 km from  
466 the coast). In addition, the ratio of  $\text{nssSO}_4^{2-}$  flux at P1 over that at P3 is 2.2, the lowest value among the  
467 ratios for the observed ions (17.2, 7.5, 26.7, 8.5, 17.4, 17.0, and 10.0 for  $\text{Cl}^-$ ,  $\text{NO}_3^-$ ,  $\text{Na}^+$ ,  $\text{NH}_4^+$ ,  $\text{K}^+$ ,  
468  $\text{Mg}^{2+}$ , and  $\text{Ca}^{2+}$ , respectively), suggesting more efficient transport of  $\text{nssSO}_4^{2-}$ . In other words,  
469 atmospheric  $\text{nssSO}_4^{2-}$  from the open ocean can be efficiently transported to at least as far inland as  
470 ~800 km from the coast (~2800 m above sea level; site P2).

471 At P1, the plots of  $\text{Cl}^-$ ,  $\text{K}^+$ ,  $\text{Mg}^{2+}$ , and  $\text{Ca}^{2+}$  versus  $\text{Na}^+$  are all close to the bulk seawater dilution line  
472 (Fig. 11), with EFs of the four species generally below 3. In addition, the slope values of the linear  
473 regression between  $\text{Na}^+$  and the four ions are close to those of seawater, suggesting a dominant source  
474 of sea salt aerosols. As for  $\text{SO}_4^{2-}$  in the snow, the proportion of  $\text{nssSO}_4^{2-}$  to  $\text{SO}_4^{2-}$  is much higher in  
475 summer (~86 %) than in winter (~27 %). All  $\text{nssSO}_4^{2-}$  in summer snow is positive, while some winter  
476 snow samples featured negative  $\text{nssSO}_4^{2-}$ , i.e.,  $\text{SO}_4^{2-}/\text{Na}^+$  ratio below the value of seawater (Fig. 4(a)),  
477 suggesting sea salt aerosols in winter from sea ice (Marion et al., 1999). In the winter snow, if all of the  
478  $\text{SO}_4^{2-}$  is from sea salt aerosols,  $\text{nssSO}_4^{2-}$  is expected to be lower than or close to zero. However, 13 out  
479 of the 17 samples classified as winter snow at P1 were characterized with positive  $\text{nssSO}_4^{2-}$ , suggesting  
480 a significant contribution from marine biogenic emissions. It is interesting that  $\text{nssSO}_4^{2-}$  has a strong  
481 negative correlation with  $\text{Na}^+$  in winter snow ( $r=0.82$ ,  $p<0.001$ ), raising two potential cases: 1) stronger  
482 winds transport more sea salt aerosols to P1 featured with depleted  $\text{SO}_4^{2-}$  from sea ice, thereby resulting



483 in low concentrations of  $\text{nssSO}_4^{2-}$  and assuming a stable  $\text{SO}_4^{2-}$  input flux from marine biogenic  
484 emissions; and/or 2) with a larger extent of sea ice and strong transport, a large sea salt flux would still  
485 result but carry less  $\text{nssSO}_4^{2-}$  from marine biogenic emissions due to the longer transport distance  
486 (Wolff et al., 2006 and references therein). If case 2) dominated  $\text{nssSO}_4^{2-}$  variations in the winter snow,  
487 lower  $\text{nssSO}_4^{2-}$  would be expected in the end than at the beginning of winter when a sea ice coverage  
488 minimum is present. The observation at P1, however, does not support this expected season trend (Fig.  
489 S2). It is most likely, then, that sea salt aerosol inputs dominate  $\text{nssSO}_4^{2-}$  variations in the winter snow  
490 instead of the marine biogenic emissions.

491 The patterns of relationships between ions and  $\text{Na}^+$  at P2 are similar to those of P1 except for  $\text{Ca}^{2+}$   
492 (Fig. 11). EFs of  $\text{Cl}^-$ ,  $\text{K}^+$ , and  $\text{Mg}^{2+}$  at P2 are  $1.5 \pm 0.2$ ,  $1.4 \pm 0.5$ , and  $1.5 \pm 0.3$  ( $\text{mean} \pm 1\sigma$ ), respectively,  
493 suggesting again a main source of sea salt aerosols. EFs of  $\text{Cl}^-$  are slightly higher in summer snow  
494 (1.57) than in winter snow (1.47), possibly indicating the presence of elevated  $\text{H}_2\text{SO}_4$  and  $\text{HNO}_3$  during  
495 summer promoting the production of  $\text{HCl}$  via R1 and R2 (discussed above).  $\text{Ca}^{2+}$  is enriched in P2  
496 (EFs =  $6.1 \pm 2.8$ ), and it remains relatively constant with increasing  $\text{Na}^+$  (Fig. 11), possibly suggesting  
497 seasonal variations in terrestrial dust inputs are insignificant. As for  $\text{SO}_4^{2-}$ , it is significantly enriched,  
498 with the EFs of  $18.6 \pm 11.4$ , and the fractions of  $\text{nssSO}_4^{2-}$  to  $\text{SO}_4^{2-}$  in summer and winter snow are 95  
499 and 89 %, respectively. The very high  $\text{SO}_4^{2-}$  to  $\text{Na}^+$  ratio in winter ( $\sim 1.6$ , versus 0.12 of bulk seawater)  
500 suggests that marine biogenic emissions dominate  $\text{SO}_4^{2-}$  other than the sea salt aerosols, different from  
501 that at P1. It is suggested that the sea salt aerosol flux from the sea ice in winter is much lower in the  
502 inland Antarctica than on the coast. Previous investigations proposed that sea salt aerosols emitted from  
503 sea ice are an important contribution to sea salt budget in central Antarctica in winter (Levine et al.,  
504 2014; Legrand et al., 2016; Legrand et al., 2017b). Here, our data indicate that marine emissions could  
505 also be an important source.

506 At P3,  $\text{Cl}^-$ ,  $\text{K}^+$ , and  $\text{Mg}^{2+}$  are correlated well with  $\text{Na}^+$  (Fig. 11), and EFs of the 3 ions are  $2.1 \pm 1.0$ ,  
507  $2.6 \pm 1.3$ , and  $2.0 \pm 0.8$ , respectively, higher than those of P2. Although the sea salt fractions of  $\text{Cl}^-$ ,  $\text{K}^+$ ,  
508 and  $\text{Mg}^{2+}$  account for most of their total budgets in the snow, the other sources can occasionally be  
509 important. On average,  $\text{nssCl}^-$  accounts for  $\sim 40$  % of the total  $\text{Cl}^-$ , suggesting that,  $\text{Cl}^-$  at Dome A is  
510 mainly from the sea salt aerosols, but the deposition of  $\text{HCl}$  is also an important contribution. This  
511 percentage is higher than that at P2 ( $\sim 30$  %), suggesting a more important role of  $\text{HCl}$  on  $\text{Cl}^-$  budget in  
512 further inland snow.  $\text{Ca}^{2+}$  is enriched noticeably at P3, with EFs of  $6.6 \pm 5.0$ , close to that of P2,  
513 suggesting the terrestrial particle mass as the primary source. In terms of  $\text{SO}_4^{2-}$ , it is enriched  
514 significantly (EFs of  $27.4 \pm 17.3$ ), and the non-sea salt fraction accounts for  $\sim 95$  % of total  $\text{SO}_4^{2-}$ ,  
515 comparable to that of P2. At P2 and P3, the negative  $\text{nssSO}_4^{2-}$  signal resulted from sea salt aerosols  
516 originated from sea ice has been completely swamped by the biogenic  $\text{SO}_4^{2-}$ , generally in line with the  
517 observation at Dome C (Udisti et al., 2012).

518 The ternary plots of  $\text{Cl}^-$ ,  $\text{Na}^+$ , and  $\text{SO}_4^{2-}$  at the three pits are shown in Fig. 12. At P1, all plots are  
519 close to the seawater composition line, suggesting the modification processes to sea salt aerosols is  
520 negligible, similar to that of coastal surface snow. Several winter snow samples at P1 show a depletion  
521 of  $\text{SO}_4^{2-}$  relative to seawater, associated with the precipitation of mirabilite during sea ice formation,  
522 while more additional  $\text{SO}_4^{2-}$  is present in summer snow (Fig. 12(a)). In general, patterns of the three  
523 ions at P2 are similar to those of P1, but with  $\text{Cl}^-$  enriched, especially in summer snow (Fig. 12(b)).  
524 Similarly, enriched  $\text{Cl}^-$  was observed at P3 (Fig. 12(c)), associated with scavenging of  $\text{HCl}$  in the  
525 atmosphere by snow. Such a pattern implies the ubiquitous modification process to sea salts in inland  
526 Antarctica throughout the year (via R1 and R2). Together with the surface snow observations (Fig. 9),



527 Cl<sup>-</sup> in the interior areas, often deviating from the seawater dilution line remarkably, is not a quantitative  
528 indicator of sea salts in snow. At P3, the data points are closer to the SO<sub>4</sub><sup>2-</sup> summit in comparison with  
529 the other two sites, possibly suggesting predominant H<sub>2</sub>SO<sub>4</sub> scavenging (e.g., Mahalinganathan et al.,  
530 2011).

531

#### 532 4.4 Interannual variations of ions in surface snow

533 As the snow sampling protocols (e.g., sampling snow depth and intervals) on the traverse are the  
534 same in different years, we can directly compare ion concentrations in surface snow collected during  
535 different campaigns. Independent samples t test showed that concentrations of Cl<sup>-</sup>, Na<sup>+</sup>, K<sup>+</sup>, Mg<sup>2+</sup>, and  
536 SO<sub>4</sub><sup>2-</sup> in surface snow are generally higher in 2015 than in the other years, while Ca<sup>2+</sup> exhibited an  
537 opposite pattern ( $p < 0.05$ ; Table S1). (2019 data are from personal communication with S. Lu, 2020)  
538 Averaged ion concentrations in surface snow collected in different campaigns are shown in Fig. 13.

539 As for the sea salt related ions in surface snow, i.e., Cl<sup>-</sup>, Na<sup>+</sup>, K<sup>+</sup>, and Mg<sup>2+</sup>, their concentrations are  
540 largely dependent on the transport strength of sea salt aerosols from the oceans, which is strongly  
541 linked to large scale atmospheric and oceanic circulation at the high southern latitudes (Goodwin et al.,  
542 2004; Russell and McGregor, 2010). We hypothesize that snow sea salt concentrations in Princess  
543 Elizabeth Land (PEL), where most of the investigation sites in this study are located (Fig. 1), are  
544 related to the variations in the sea level pressure over the Southern Indian Ocean, specifically the  
545 Southern Indian Ocean low (SIOL), a quasi-stationary climatological feature located north of Prydz  
546 Bay (Xiao et al., 2004). To test this hypothesis, interannual variation in the SIOL during the study  
547 period was examined with the aid of the ERA-interim reanalysis. To quantify the strength of the SIOL,  
548 the circulation indices of a closed pressure system, including the area index (S) and strength index (P),  
549 were calculated following Wang et al. (2007). Considering that the sampling time was January and  
550 February, the austral summertime mean sea level pressure was used to calculate the circulation indices  
551 in each year (Fig. S3). It is shown that the SIOL is stronger in the austral summer of 2014/2015, i.e.,  
552 the larger area and the greater strength of SIOL (Fig. S3(f)). A significant correlation was found  
553 between the area index of SIOL (S) and Na<sup>+</sup> ( $r=0.89$ ,  $p=0.03$ ; Fig. 13(a)). Accordingly, the higher  
554 concentrations of sea salts observed in 2015 can, at least in part, be explained by the SIOL anomaly.  
555 Indeed, the marine air mass intrusion into the continent is associated with large scale boundary-layer  
556 turbulence over the ocean or blocking anticyclones (Naithani et al., 2002; Goodwin et al., 2004), and  
557 higher snow sea salt concentrations in coastal PEL were generally connected to the deepening of SIOL  
558 (Xiao et al., 2004).

559 Similar to the temporal patterns of sea salts, higher SO<sub>4</sub><sup>2-</sup> (and nssSO<sub>4</sub><sup>2-</sup>) concentrations were also  
560 observed in 2015. This is likely associated with the fact that SO<sub>4</sub><sup>2-</sup> in surface snow is mainly from  
561 marine biogenic emissions, and a stronger SIOL would also promote the transport of SO<sub>4</sub><sup>2-</sup>.  
562 Interestingly, Ca<sup>2+</sup> exhibits the lowest concentration in 2015, which may be related to that Ca<sup>2+</sup> is  
563 mainly originated from the mid-latitude terrestrial particle mass, instead of the Southern Ocean  
564 emissions. A stronger polar low (e.g., SIOL) usually corresponds to strengthening westerly winds, and  
565 thereby would result in weaker meridional transport from the mid-latitudes (Marshall, 2003; Goodwin  
566 et al., 2004; Jones et al., 2009).

567 It is noted that the observation covers a relatively short period of time, and changes in snow  
568 accumulation rate and transport strength from year to year are also likely to influence the variability of  
569 ions on an interannual timescale. Thus, there is still uncertainty on the relationships between ion  
570 concentrations and the SIOL. During the observation period (2011-2019), however, the SIOL is likely



571 an important factor influencing the interannual variability of major ions in surface snow on the  
572 traverse.

573

## 574 **5 Conclusions**

575 Surface snow and snow pit samples collected on a traverse from coastal Zhongshan Station to the ice  
576 sheet summit, East Antarctica, during five campaigns were used to comprehensively investigate spatial  
577 and temporal variations in snow chemistry. It is shown that  $\text{Cl}^-$ ,  $\text{Na}^+$ ,  $\text{K}^+$ , and  $\text{Mg}^{2+}$  concentrations are  
578 high within the narrow coastal region, falling off strongly further inland, while  $\text{NO}_3^-$  exhibits an  
579 opposite trend and no clear spatial trends were found for  $\text{SO}_4^{2-}$ ,  $\text{NH}_4^+$ , and  $\text{Ca}^{2+}$ . In inland snow,  $\text{Cl}^-$ ,  $\text{K}^+$ ,  
580 and  $\text{Mg}^{2+}$  are slightly enriched relative to  $\text{Na}^+$  with respect to the composition of seawater. The  
581 enrichment of  $\text{Cl}^-$  is likely associated with the deposition of HCl produced from dechlorination of sea  
582 salt aerosols, and enriched  $\text{K}^+$  and  $\text{Mg}^{2+}$  are possibly linked to terrestrial particle mass.  $\text{Ca}^{2+}$  and  $\text{SO}_4^{2-}$   
583 are significantly enriched versus  $\text{Na}^+$ , and terrestrial dust mass and marine biogenic emissions are  
584 responsible for the enrichments respectively. Snow  $\text{NH}_4^+$  is related to marine biological activities, and  
585 multivariate statistical analysis suggests, at least in part, the  $\text{NH}_4^+$  transport is via free troposphere.

586 In coastal snow pit, parts of the winter snow showed a depletion of  $\text{SO}_4^{2-}$  versus  $\text{Na}^+$ , indicating sea  
587 salt aerosols sourced from sea ice. In the interior areas, although sea salt aerosols originated from sea  
588 ice contribute to a significant depletion of  $\text{SO}_4^{2-}$ , the negative  $\text{nssSO}_4^{2-}$  signal has been completely  
589 swamped by the contribution from biogenic  $\text{SO}_4^{2-}$ . In addition,  $\text{Cl}^-$  in the snow is more enriched in  
590 summer than in winter, possibly related to more HCl formation due to elevated acid concentrations  
591 during summertime. Ternary plots of  $\text{Cl}^-$ ,  $\text{Na}^+$  and  $\text{SO}_4^{2-}$  in snow suggest the modification process to  
592 sea salts is negligible on the coast, while the degree of modification to sea salts is higher in inland  
593 throughout the year, which results in  $\text{Cl}^-$  not being a quantitative indicator of sea salts. Ion flux  
594 assessment suggests an efficient transport of  $\text{nssSO}_4^{2-}$  to at least as far inland as the ~2800 m contour  
595 line. With the aid of reanalysis, it is found that the interannual variations in ion concentrations in  
596 surface snow are likely connected to changes in the Southern Indian Ocean low from year to year.

597

598 **Data availability.** This dataset, chemical data on ion concentrations in snow on the traverse from coast  
599 (Zhongshan Station) to Dome A, is in the process of being hosted on a public server by the Chinese  
600 National Arctic and Antarctic Data Center (<https://www.chinare.org.cn/>).

601

602 **Author contributions.** GS, ZC, YL and BS designed the experiments and GS, HM, ZH, CA, SJ, TM,  
603 JY, DW and SL carried them out. GS and MH prepared the manuscript with contributions from all  
604 co-authors.

605

606 **Competing interests.** The authors declare that they have no conflict of interest.

607

## 608 **Acknowledgements**

609 This research was supported by the National Science Foundation of China (Grant Nos. 41922046 and  
610 41576190 to GS; Grant No. 41876225 to HM) and the National Key Research and Development  
611 Program of China (Grant No. 2016YFA0302204 to GS). The authors are grateful to the CHINARE  
612 inland members for logistic support and assistance.

613



614 **References**

- 615 Abram, N.J., Wolff, E.W., Curran, M.A.J., 2013. A review of sea ice proxy information from polar ice  
616 cores. *Quaternary Sci. Rev.* 79, 168-183.
- 617 Albert, M.R., Shultz, E.F., 2002. Snow and firn properties and air–snow transport processes at Summit,  
618 Greenland. *Atmos. Environ.* 36, 2789-2797.
- 619 Basile, I., Grousset, F.E., Revel, M., Petit, J.R., Biscaye, P.E., Barkov, N.I., 1997. Patagonian origin of  
620 glacial dust deposited in East Antarctica (Vostok and Dome C) during glacial stages 2, 4 and 6. *Earth  
621 Planet. Sci. Lett.* 146, 573-589.
- 622 Bertler, N., Mayewski, P.A., Aristarain, A., Barrett, P., Becagli, S., Bernardo, R., Bo, S., Xiao, C.,  
623 Curran, M., Qin, D., 2005. Snow chemistry across Antarctica. *Ann. Glaciol.* 41, 167-179.
- 624 Björkman, M.P., Vega, C.P., Kühnel, R., Spataro, F., Ianniello, A., Esposito, G., Kaiser, J., Marca, A.,  
625 Hodson, A., Isaksson, E., 2014. Nitrate post-depositional processes in Svalbard surface snow. *J.  
626 Geophys. Res.* 119, 12953-12976.
- 627 Bondiotti, E.A., Papastefanou, C., 1993. Estimates of residence times of sulfate aerosols in ambient air.  
628 *Sci. Total Environ.* 136, 25-31.
- 629 Bowen, H.J.M., 1979. *Environmental Chemistry of the Elements*. Academic Press, London.
- 630 Caiazza, L., Becagli, S., Frosini, D., Giardi, F., Severi, M., Traversi, R., Udisti, R., 2016. Spatial and  
631 temporal variability of snow chemical composition and accumulation rate at Talos Dome site (East  
632 Antarctica). *Sci. Total Environ.* 550, 418.
- 633 Cole-Dai, J., Ferris, D.G., Lanciki, A.L., Savarino, J., Thiemens, M.H., McConnell, J.R., 2013. Two  
634 likely stratospheric volcanic eruptions in the 1450s C.E. found in a bipolar, subannually dated 800 year  
635 ice core record. *J. Geophys. Res.* 118, 7459-7466.
- 636 Cole-Dai, J., Mosley-Thompson, E., Thompson, L.G., 1997. Annually resolved southern hemisphere  
637 volcanic history from two Antarctic ice cores. *J. Geophys. Res.* 102, 16761–16771.
- 638 Cole-Dai, J., Mosley-Thompson, E., Wight, S.P., Thompson, L.G., 2000. A 4100-year record of  
639 explosive volcanism from an East Antarctica ice core. *J. Geophys. Res.* 105, 24431-24442.
- 640 Cunningham, J., Waddington, E., 1993. Air flow and dry deposition of non-sea salt sulfate in polar firn:  
641 paleoclimatic implications. *Atmospheric Environment. Part A. General Topics* 27, 2943-2956.
- 642 Das, I., Bell, R.E., Scambos, T.A., Wolovick, M., Creyts, T.T., Studinger, M., Frearson, N., Nicolas, J.P.,  
643 Lenaerts, J.T., van den Broeke, M.R., 2013. Influence of persistent wind scour on the surface mass  
644 balance of Antarctica. *Nat. Geosci.* 6, 367-371.
- 645 Davis, D.D., Eisele, F., Chen, G., 2004. An overview of ISCAT. *Atmos. Environ.*, 5363-5373.
- 646 Delmas, R., 1992. Environmental information from ice cores. *Rev. Geophys.* 30, 1-21.
- 647 Delmonte, B., Baroni, C., Andersson, P., Narcisi, B., Salvatore, M.C., Petit, J., Scarchilli, C., Frezzotti,  
648 M., Albani, S., Maggi, V., 2013. Modern and Holocene aeolian dust variability from Talos Dome  
649 (Northern Victoria Land) to the interior of the Antarctic ice sheet. *Quaternary Sci. Rev.* 64, 76-89.
- 650 Ding, M., Xiao, C., Li, C., Qin, D., Jin, B., Shi, G., Xie, A., Cui, X., 2015. Surface mass balance and its  
651 climate significance from the coast to Dome A, East Antarctica. *Science China Earth Sciences* 58,  
652 1787-1797.
- 653 Ding, M., Xiao, C., Li, Y., Ren, J., Hou, S., Jin, B., Sun, B., 2011. Spatial variability of surface mass  
654 balance along a traverse route from Zhongshan station to Dome A, Antarctica. *J. Glaciol.* 57, 658-666.
- 655 Ding, M., Xiao, C., Yang, Y., Wang, Y., Li, C., Yuan, N., Shi, G., Sun, W., Ming, J., 2016.  
656 Re-assessment of recent (2008–2013) surface mass balance over Dome Argus, Antarctica. *Polar Res.*  
657 35, 26133.



- 658 Dixon, D.A., Mayewski, P.A., Korotkikh, E., Sneed, S.B., Handley, M.J., Introne, D.S., Scambos, T.A.,  
659 2013. Variations in snow and firn chemistry along US ITASE traverses and the effect of surface glazing.  
660 *Cryosphere* 7, 515-535.
- 661 Du, Z., Xiao, C., Ding, M., Li, C., 2018. Identification of multiple natural and anthropogenic sources of  
662 dust in snow from Zhongshan Station to Dome A, East Antarctica. *J. Glaciol.* 64, 855-865.
- 663 Du, Z., Xiao, C., Handley, M.J., Mayewski, P.A., Li, C., Liu, S., Ma, X., Yang, J., 2019. Fe variation  
664 characteristics and sources in snow samples along a traverse from Zhongshan Station to Dome A, East  
665 Antarctica. *Sci. Total Environ.*
- 666 EPICA Community Members, 2004. Eight glacial cycles from an Antarctic ice core. *Nature* 429,  
667 623-628.
- 668 Erbland, J., Vicars, W., Savarino, J., Morin, S., Frey, M., Frosini, D., Vince, E., Martins, J., 2013.  
669 Air-snow transfer of nitrate on the East Antarctic Plateau - Part 1: Isotopic evidence for a photolytically  
670 driven dynamic equilibrium in summer. *Atmos. Chem. Phys.* 13, 6403-6419.
- 671 Finlayson-Pitts, B.J., 2003. The tropospheric chemistry of sea salt: a molecular-level view of the  
672 chemistry of NaCl and NaBr. *Chem. Rev.* 103, 4801-4822.
- 673 Frey, M.M., Norris, S.J., Brooks, I.M., Anderson, P.S., Nishimura, K., Yang, X., Jones, A.E., Nerentorp  
674 Mastromonaco, M.G., Jones, D.H., Wolff, E.W., 2020. First direct observation of sea salt aerosol  
675 production from blowing snow above sea ice. *Atmos. Chem. Phys.* 20, 2549-2578.
- 676 Goodwin, I., Van Ommen, T., Curran, M., Mayewski, P., 2004. Mid latitude winter climate variability  
677 in the South Indian and southwest Pacific regions since 1300 AD. *Clim. Dynam.* 22, 783-794.
- 678 Gragnani, R., Smiraglia, C., Stenni, B., Torcini, S., 1998. Chemical and isotopic profiles from snow  
679 pits and shallow firn cores on Campbell Glacier, northern Victoria Land, Antarctica. *Ann. Glaciol.* 27,  
680 679-684.
- 681 Hara, K., Nakazawa, F., Fujita, S., Fukui, K., Enomoto, H., Sugiyama, S., 2014. Horizontal  
682 distributions of aerosol constituents and their mixing states in Antarctica during the JASE traverse.  
683 *Atmos. Chem. Phys.* 14, 10211-10230.
- 684 Hara, K., Osada, K., Yamanouchi, T., 2013. Tethered balloon-borne aerosol measurements: seasonal  
685 and vertical variations of aerosol constituents over Syowa Station, Antarctica. *Atmos. Chem. Phys.* 13,  
686 9119-9139.
- 687 Holland, P.R., Bruneau, N., Enright, C., Losch, M., Kurtz, N.T., Kwok, R., 2014. Modeled Trends in  
688 Antarctic Sea Ice Thickness. *J. Climate* 27, 3784-3801.
- 689 Hou, S., Li, Y., Xiao, C., Ren, J., 2007. Recent accumulation rate at Dome A, Antarctica. *Chin. Sci.*  
690 *Bull.* 52, 428-431.
- 691 Ishino, S., Hattori, S., Savarino, J., Jourdain, B., Preunkert, S., Legrand, M., Caillon, N., Barbero, A.,  
692 Kuribayashi, K., Yoshida, N., 2017. Seasonal variations of triple oxygen isotopic compositions of  
693 atmospheric sulfate, nitrate and ozone at Dumont d'Urville, coastal Antarctica. *Atmos. Chem. Phys.* 17,  
694 1-25.
- 695 Jiang, S., Cole-Dai, J., Li, Y., Ferris, D.G., Ma, H., An, C., Shi, G., Sun, B., 2012. A detailed 2840 year  
696 record of explosive volcanism in a shallow ice core from Dome A, East Antarctica. *J. Glaciol.* 58,  
697 65-75.
- 698 Johnson, M., Sanders, R., Avgoustidi, V., Lucas, M., Brown, L., Hansell, D., Moore, M., Gibb, S., Liss,  
699 P., Jickells, T., 2007. Ammonium accumulation during a silicate-limited diatom bloom indicates the  
700 potential for ammonia emission events. *Mar. Chem.* 106, 63-75.
- 701 Jones, A.E., Wolff, E.W., Ames, D., Bauguitte, S.-B., Clemmshaw, K., Fleming, Z., Mills, G.,



- 702 Saiz-Lopez, A., Salmon, R.A., Sturges, W., 2011. The multi-seasonal NO<sub>y</sub> budget in coastal Antarctica  
703 and its link with surface snow and ice core nitrate: results from the CHABLIS campaign. *Atmos. Chem.*  
704 *Phys.* 11, 9271-9285.
- 705 Jones, J.M., Fogt, R.L., Widmann, M., Marshall, G.J., Jones, P.D., Visbeck, M., 2009. Historical SAM  
706 Variability. Part I: Century-Length Seasonal Reconstructions. *J. Climate* 22, 5319-5345.
- 707 Jouzel, J., Masson-Delmotte, V., Cattani, O., Dreyfus, G., Falourd, S., Hoffmann, G., Minster, B.,  
708 Nouet, J., Barnola, J.M., Chappellaz, J., Fischer, H., Gallet, J.C., Johnsen, S., Leuenberger, M.,  
709 Loulergue, L., Luethi, D., Oerter, H., Parrenin, F., Raisbeck, G., Raynaud, D., Schilt, A., Schwander, J.,  
710 Selmo, E., Souchez, R., Spahni, R., Stauffer, B., Steffensen, J.P., Stenni, B., Stocker, T.F., Tison, J.L.,  
711 Werner, M., Wolff, E.W., 2007. Orbital and Millennial Antarctic Climate Variability over the Past  
712 800,000 Years. *Science* 317, 793-796.
- 713 Kärkäs, E., Teinilä, K., Virkkula, A., Aurela, M., 2005. Spatial variations of surface snow chemistry  
714 during two austral summers in western Dronning Maud Land, Antarctica. *Atmos. Environ.* 39,  
715 1405-1416.
- 716 Kaufmann, P., Fundel, F., Fischer, H., Bigler, M., Ruth, U., Udisti, R., Hansson, M., De Angelis, M.,  
717 Barbante, C., Wolff, E.W., 2010. Ammonium and non-sea salt sulfate in the EPICA ice cores as  
718 indicator of biological activity in the Southern Ocean. *Quaternary Sci. Rev.* 29, 313-323.
- 719 Keene, W.C., Maring, H., Maben, J.R., Kieber, D.J., Pszenny, A.A., Dahl, E.E., Izaguirre, M.A., Davis,  
720 A.J., Long, M.S., Zhou, X., 2007. Chemical and physical characteristics of nascent aerosols produced  
721 by bursting bubbles at a model air - sea interface. *J. Geophys. Res.* 112.
- 722 Khodzher, T.V., Golobokova, L.P., Osipov, E.Y., Shibaev, Y.A., Lipenkov, V.Y., Osipova, O.P., Petit,  
723 J.R., 2014. Spatial-temporal dynamics of chemical composition of surface snow in East Antarctica  
724 along the Progress station-Vostok station transect. *Cryosphere* 8, 931-939.
- 725 Krinner, G., Genthon, C., 2003. Tropospheric transport of continental tracers towards Antarctica under  
726 varying climatic conditions. *Tellus B* 55, 54-70.
- 727 Krinner, G., Petit, J.R., Delmonte, B., 2010. Altitude of atmospheric tracer transport towards Antarctica  
728 in present and glacial climate. *Quaternary Sci. Rev.* 29, 274-284.
- 729 Lee, H.-M., Henze, D.K., Alexander, B., Murray, L.T., 2014. Investigating the sensitivity of  
730 surface-level nitrate seasonality in Antarctica to primary sources using a global model. *Atmos. Environ.*  
731 89, 757-767.
- 732 Legrand, M., Preunkert, S., Weller, R., Zipf, L., Elsässer, C., Merchel, S., Rugel, G., Wagenbach, D.,  
733 2017a. Year-round record of bulk and size-segregated aerosol composition in central Antarctica  
734 (Concordia site) – Part 2: Biogenic sulfur (sulfate and methanesulfonate) aerosol. *Atmos. Chem. Phys.*  
735 17, 14055-14073.
- 736 Legrand, M., Preunkert, S., Wolff, E., Weller, R., Jourdain, B., Wagenbach, D., 2017b. Year-round  
737 records of bulk and size-segregated aerosol composition in central Antarctica (Concordia site) – Part 1:  
738 Fractionation of sea-salt particles. *Atmos. Chem. Phys.* 17, 14039-14054.
- 739 Legrand, M., Yang, X., Preunkert, S., Theys, N., 2016. Year-round records of sea salt, gaseous, and  
740 particulate inorganic bromine in the atmospheric boundary layer at coastal (Dumont d'Urville) and  
741 central (Concordia) East Antarctic sites. *J. Geophys. Res.* 121, 2015JD024066.
- 742 Legrand, M.R., Delmas, R.J., 1988. Soluble impurities in four Antarctic ice cores over the last 30,000  
743 years. *Ann. Glaciol.* 10, 116-120.
- 744 Levine, J., Yang, X., Jones, A., Wolff, E., 2014. Sea salt as an ice core proxy for past sea ice extent: A  
745 process - based model study. *J. Geophys. Res.* 119, 5737-5756.



- 746 Li, C., Xiao, C., Shi, G., Ding, M., Kang, S., Zhang, L., Hou, S., Sun, B., Qin, D., Ren, J., 2015.  
747 Spatiotemporal variations of monocarboxylic acids in snow layers along a transect from Zhongshan  
748 Station to Dome A, eastern Antarctica. *Atmos. Res.* 158-159, 79-87.
- 749 Li, C., Xiao, C., Shi, G., Ding, M., Qin, D., Ren, J., 2016. Spatial and temporal variability of  
750 marine-origin matter along a transect from Zhongshan Station to Dome A, Eastern Antarctica. *J.*  
751 *Environ. Sci.* 46, 190-202.
- 752 Libois, Q., Picard, G., Arnaud, L., Morin, S., Brun, E., 2014. Modeling the impact of snow drift on the  
753 decameter - scale variability of snow properties on the Antarctic Plateau. *J. Geophys. Res.* 119,  
754 11,662-611,681.
- 755 Mahalinganathan, K., Thamban, M., 2016. Potential genesis and implications of calcium nitrate in  
756 Antarctic snow. *Cryosphere* 10, 825-836.
- 757 Mahalinganathan, K., Thamban, M., Laluraj, C.M., Redkar, B.L., 2011. Relation between surface  
758 topography and sea-salt snow chemistry from Princess Elizabeth Land, East Antarctica. *Cryosphere* 6,  
759 505-515.
- 760 Marion, G., Farren, R., Komrowski, A., 1999. Alternative pathways for seawater freezing. *Cold Reg.*  
761 *Sci. Technol.* 29, 259-266.
- 762 Marshall, G.J., 2003. Trends in the Southern Annular Mode from observations and reanalyses. *J.*  
763 *Climate* 16, 4134-4143.
- 764 Mayewski, P.A., Carleton, A.M., Birkel, S.D., Dixon, D., Kurbatov, A.V., Korotkikh, E., McConnell, J.,  
765 Curran, M., Cole-Dai, J., Jiang, S., Plummer, C., Vance, T., Maasch, K.A., Sneed, S.B., Handley, M.,  
766 2017. Ice core and climate reanalysis analogs to predict Antarctic and Southern Hemisphere climate  
767 changes. *Quaternary Sci. Rev.* 155, 50-66.
- 768 Morin, S., Sander, R., Savarino, J., 2011. Simulation of the diurnal variations of the oxygen isotope  
769 anomaly ( $\Delta^{17}\text{O}$ ) of reactive atmospheric species. *Atmos. Chem. Phys.* 11, 3653-3671.
- 770 Mulvaney, R., Wolff, E., 1994. Spatial variability of the major chemistry of the Antarctic ice sheet. *Ann.*  
771 *Glaciol.* 20, 440-447.
- 772 Naithani, J., Gallée, H., Schayes, G., 2002. Marine air intrusion into the Adelie Land sector of East  
773 Antarctica: A study using the regional climate model (MAR). *J. Geophys. Res.* 107, ACL 6-1-ACL  
774 6-16.
- 775 Nozaki, Y., 2001. Element distribution overview, in: Steele, J., Thorpe, S., Turekian, K.K. (Eds.),  
776 *Encyclopedia of Ocean Sciences.* Academic Press, London, pp. 840-845.
- 777 Pasteris, D.R., McConnell, J.R., Das, S.B., Criscitiello, A.S., Evans, M.J., Maselli, O.J., Sigl, M.,  
778 Layman, L.C.J.D., 2014. Seasonally resolved ice core records from West Antarctica indicate a sea ice  
779 source of sea-salt aerosol and a biomass burning source of ammonium. *J. Geophys. Res.* 119,  
780 9168-9182.
- 781 Pasteris, D.R., McConnell, J.R., Edwards, R., 2012. High-resolution, continuous method for  
782 measurement of acidity in ice cores. *Environ. Sci. Technol.* 46, 1659.
- 783 Proposito, M., Becagli, S., Castellano, E., Flora, O., Genoni, L., Gragnani, R., Stenni, B., Traversi, R.,  
784 Udasti, R., Frezzotti, M., 2002. Chemical and isotopic snow variability along the 1998 ITASE traverse  
785 from Terra Nova Bay to Dome C, East Antarctica. *Ann. Glaciol.* 35, 187-194.
- 786 Qin, D., Zeller, E.J., Dreschhoff, G.A., 1992. The distribution of nitrate content in the surface snow of  
787 the Antarctic Ice Sheet along the route of the 1990 International Trans-Antarctica Expedition. *J.*  
788 *Geophys. Res.* 97, 6277-6284.
- 789 Röthlisberger, R., Mulvaney, R., Wolff, E.W., Hutterli, M.A., Bigler, M., De Angelis, M., Hansson,



- 790 M.E., Steffensen, J.P., Udisti, R., 2003. Limited dechlorination of sea-salt aerosols during the last  
791 glacial period: Evidence from the European Project for Ice Coring in Antarctica (EPICA) Dome C ice  
792 core. *J. Geophys. Res.* 108, 4526, doi:4510.1029/2003JD003604.
- 793 Röthlisberger, R., Mulvaney, R., Wolff, E.W., Hutterli, M.A., Bigler, M., Sommer, S., Jouzel, J., 2002.  
794 Dust and sea salt variability in central East Antarctica (Dome C) over the last 45 kyrs and its  
795 implications for southern high-latitude climate. *Geophys. Res. Lett.* 29, 24-21-24-24.
- 796 Rankin, A.M., Wolff, E.W., 2000. Ammonium and potassium in snow around an emperor penguin  
797 colony. *Antarct. Sci.* 12, 154-159.
- 798 Russell, A., McGregor, G.R., 2010. Southern hemisphere atmospheric circulation: impacts on Antarctic  
799 climate and reconstructions from Antarctic ice core data. *Climate Change* 99, 155-192.
- 800 Saltzman, E.S., 1995. Ocean/atmosphere cycling of dimethylsulfide, in: Delmas, R.J. (Ed.), *Ice core*  
801 *studies of global biogeochemical cycles*. Springer, Berlin, pp. 65-89.
- 802 Sato, K., Takenaka, N., Bandow, H., Maeda, Y., 2008. Evaporation loss of dissolved volatile substances  
803 from ice surfaces. *J. Phys. Chem.* 112, 7600-7607.
- 804 Savarino, J., Kaiser, J., Morin, S., Sigman, D.M., Thiemens, M.H., 2007. Nitrogen and oxygen isotopic  
805 constraints on the origin of atmospheric nitrate in coastal Antarctica. *Atmos. Chem. Phys.* 7,  
806 1925-1945.
- 807 Severi, M., Becagli, S., Caiazzo, L., Ciardini, V., Colizza, E., Giardi, F., Mezgec, K., Sarchilli, C.,  
808 Stenni, B., Thomas, E.R., Traversi, R., Udisti, R., 2017. Sea salt sodium record from Talos Dome (East  
809 Antarctica) as a potential proxy of the Antarctic past sea ice extent. *Chemosphere* 177, 266-274.
- 810 Severi, M., Becagli, S., Castellano, E., Morganti, A., Traversi, R., Udisti, R., 2009. Thirty years of  
811 snow deposition at Talos Dome (Northern Victoria Land, East Antarctica): Chemical profiles and  
812 climatic implications. *Microchem. J.* 92, 15-20.
- 813 Shi, G., Buffen, A.M., Hastings, M.G., Li, C., Ma, H., Li, Y., Sun, B., An, C., Jiang, S., 2015.  
814 Investigation of post-depositional processing of nitrate in East Antarctic snow: isotopic constraints on  
815 photolytic loss, re-oxidation, and source inputs. *Atmos. Chem. Phys.* 15, 9435-9453.
- 816 Shi, G., Buffen, A.M., Ma, H., Hu, Z., Sun, B., Li, C., Yu, J., Ma, T., An, C., Jiang, S., Li, Y., Hastings,  
817 M.G., 2018a. Distinguishing summertime atmospheric production of nitrate across the East Antarctic  
818 Ice Sheet. *Geochim. Cosmochim. Acta* 231, 1-14.
- 819 Shi, G., Hastings, M.G., Yu, J., Ma, T., Hu, Z., An, C., Li, C., Ma, H., Jiang, S., Li, Y., 2018b. Nitrate  
820 deposition and preservation in the snowpack along a traverse from coast to the ice sheet summit (Dome  
821 A) in East Antarctica. *The Cryosphere* 12, 1177-1194.
- 822 Shi, G., Li, Y., Jiang, S., An, C., Ma, H., Sun, B., Wang, Y., 2012. Large-scale spatial variability of  
823 major ions in the atmospheric wet deposition along the China Antarctica transect (31° N~ 69° S). *Tellus*  
824 *B* 64, 17134.
- 825 Shi, G., Wang, X.-C., Li, Y., Trengove, R., Hu, Z., Mi, M., Li, X., Yu, J., Hunter, B., He, T., 2019.  
826 Organic tracers from biomass burning in snow from the coast to the ice sheet summit of East Antarctica.  
827 *Atmos. Environ.* 201, 231-241.
- 828 Suzuki, T., Iizuka, Y., Matsuoka, K., Furukawa, T., Kamiyama, K., Watanabe, O., 2002. Distribution of  
829 sea salt components in snow cover along the traverse route from the coast to Dome Fuji station 1000  
830 km inland at east Dronning Maud Land, Antarctica. *Tellus B Chemical and Physical Meteorology* 54,  
831 407-411.
- 832 Traversi, R., Becagli, S., Castellano, E., Cerri, O., Morganti, A., Severi, M., Udisti, R., 2009. Study of  
833 Dome C site (East Antarctica) variability by comparing chemical stratigraphies. *Microchem. J.* 92, 7-14.



834 Traversi, R., Becagli, S., Castellano, E., Largiuni, O., Migliori, A., Severi, M., Frezzotti, M., Udisti, R.,  
835 2004. Spatial and temporal distribution of environmental markers from Coastal to Plateau areas in  
836 Antarctica by firm core chemical analysis. *Int. J. Environ. Anal. Chem.* 84, 457-470.  
837 Udisti, R., Becagli, S., Benassai, S., Castellano, E., Fattori, I., Innocenti, M., Migliori, A., Traversi, R.,  
838 2004. Atmosphere-snow interaction by a comparison between aerosol and uppermost snow layers  
839 composition at Dome Concordia (East Antarctica). *Ann. Glaciol.* 39, 53-61(59).  
840 Udisti, R., Dayan, U., Becagli, S., Busetto, M., Frosini, D., Legrand, M., Lucarelli, F., Preunkert, S.,  
841 Severi, M., Traversi, R., 2012. Sea spray aerosol in central Antarctica. Present atmospheric behaviour  
842 and implications for paleoclimatic reconstructions. *Atmos. Environ.* 52, 109-120.  
843 Virkkula, A., Teinilä, K., Hillamo, R., Kerminen, V.M., Saarikoski, S., Aurela, M., Koponen, I.K.,  
844 Kulmala, M., 2006. Chemical size distributions of boundary layer aerosol over the Atlantic Ocean and  
845 at an Antarctic site. *Atmos. Chem. Phys.* 6, 303-310.  
846 Wagenbach, D., 1996. Coastal Antarctica: Atmospheric chemical composition and atmospheric  
847 transport, in: Wolff, E.W., Bales, R.C. (Eds.), *Chemical Exchange between the Atmosphere and polar*  
848 *snow*. Springer-Verlag, New York, pp. 173-199.  
849 Wagenbach, D., Ducroz, F., Mulvaney, R., Keck, L., Minikin, A., Legrand, M., Hall, J.S., Wolff, E.W.,  
850 1998a. Sea-salt aerosol in coastal Antarctic regions. *J. Geophys. Res.* 103, 10961-10974.  
851 Wagenbach, D., Legrand, M., Fischer, H., Pichlmayer, F., Wolff, E.W., 1998b. Atmospheric  
852 near-surface nitrate at coastal Antarctic sites. *J. Geophys. Res.* 103, 11007-11020.  
853 Wagon, P., Delmas, R.J., Legrand, M., 1999. Loss of volatile acid species from the upper firm layers at  
854 Vostok, Antarctica. *J. Geophys. Res.* 104, 3423-3431.  
855 Wang, P., Lu, C., Guan, Z., Li, S., Yao, J., Yan, L., 2007. Definition and Calculation of Three  
856 Circulation Indices for Closed Pressure Systems. *Journal of Nanjing Institute of Meteorolog* 030,  
857 730-735.  
858 Wolff, E.W., Barbante, S., Becagle, S., Bigler, M., Boutron, C.F., Castellano, E., de Angelis, M.,  
859 Federer, U., 2010. Changes in environment over the last 800,000 years from chemical analysis of the  
860 EPICA Dome C ice core. *Quaternary Sci. Rev.* 29, 285-295.  
861 Wolff, E.W., Fischer, H., Fundel, F., Ruth, U., Twarloh, B., Littot, G.C., Mulvaney, R., Röthlisberger,  
862 R., de Angelis, M., Boutron, C.F., Hansson, M., Jonsell, U., Hutterli, M.A., Lambert, F., Kaufmann, P.,  
863 Stauffer, B., Stocker, T.F., Steffensen, J.P., Bigler, M., Siggaard-Andersen, M.L., Udisti, R., Becagli, S.,  
864 Castellano, E., Severi, M., Wagenbach, D., Barbante, C., Gabrielli, P., Gaspari, V., 2006. Southern  
865 Ocean sea-ice extent, productivity and iron flux over the past eight glacial cycles. *Nature* 440, 491-496.  
866 Wolff, E.W., Rankin, A.M., Röthlisberger, R., 2003. An ice core indicator of Antarctic sea ice  
867 production? *Geophys. Res. Lett.* 30, doi:10.1029/2003GL018454.  
868 Xiao, C., Mayewski, P.A., Qin, D., Li, Z., Zhang, M., Yan, Y., 2004. Sea level pressure variability over  
869 the southern Indian Ocean inferred from a glaciochemical record in Princess Elizabeth Land, east  
870 Antarctica. *J. Geophys. Res.* 109, doi:10.1029/2003JD004065.  
871 Zhao, L., Moore, J.C., Sun, B., Tang, X., Guo, X., 2018. Where is the 1-million-year-old ice at Dome A?  
872 *The Cryosphere* 12, 1651-1663.  
873  
874



875 **Table 1** Rotated component matrix of the major ions in surface snow. (Extraction method: principal  
876 component analysis. Rotation method: varimax with Kaiser normalization. Rotation converged in 4  
877 iterations.) Factor loadings were calculated from the eigenvalues of the three components and their  
878 corresponding eigenvectors, and the values greater than 0.7 are shaded.

Chemical ions	PC1	PC2	PC3	Communalities
Cl <sup>-</sup>	0.93	-0.01	0.27	0.93
NO <sub>3</sub> <sup>-</sup>	0.04	-0.06	0.95	0.90
SO <sub>4</sub> <sup>2-</sup>	0.55	0.08	0.42	0.49
Na <sup>+</sup>	0.98	-0.01	-0.06	0.96
NH <sub>4</sub> <sup>+</sup>	0.10	0.81	0.04	0.66
K <sup>+</sup>	0.71	0.25	0.12	0.57
Mg <sup>2+</sup>	0.96	0.05	-0.09	0.92
Ca <sup>2+</sup>	0.03	0.79	-0.07	0.62
Initial eigenvalues	3.67	1.33	1.06	
Percentage of variance	46	17	13	
Cumulative percent	46	63	76	

879  
880



881 **Table 2** Pearson correlation matrix of major ions in surface snow

	Cl <sup>-</sup>	NO <sub>3</sub> <sup>-</sup>	SO <sub>4</sub> <sup>2-</sup>	Na <sup>+</sup>	NH <sub>4</sub> <sup>+</sup>	K <sup>+</sup>	Mg <sup>2+</sup>	Ca <sup>2+</sup>
Cl <sup>-</sup>	1.00	0.24**	0.47**	0.94**	0.05	0.74**	0.91**	0.09
NO <sub>3</sub> <sup>-</sup>		1.00	0.21**	-0.02	-0.04	0.09*	-0.04	-0.05
SO <sub>4</sub> <sup>2-</sup>			1.00	0.34**	0.08	0.30**	0.31**	0.03
Na <sup>+</sup>				1.00	0.05	0.77**	0.98**	0.12*
NH <sub>4</sub> <sup>+</sup>					1.00	0.19**	0.10*	0.30**
K <sup>+</sup>						1.00	0.75**	0.15**
Mg <sup>2+</sup>							1.00	0.15**
Ca <sup>2+</sup>								1.00

882 \*\* . Correlation is significant at the 0.01 level (2-tailed).

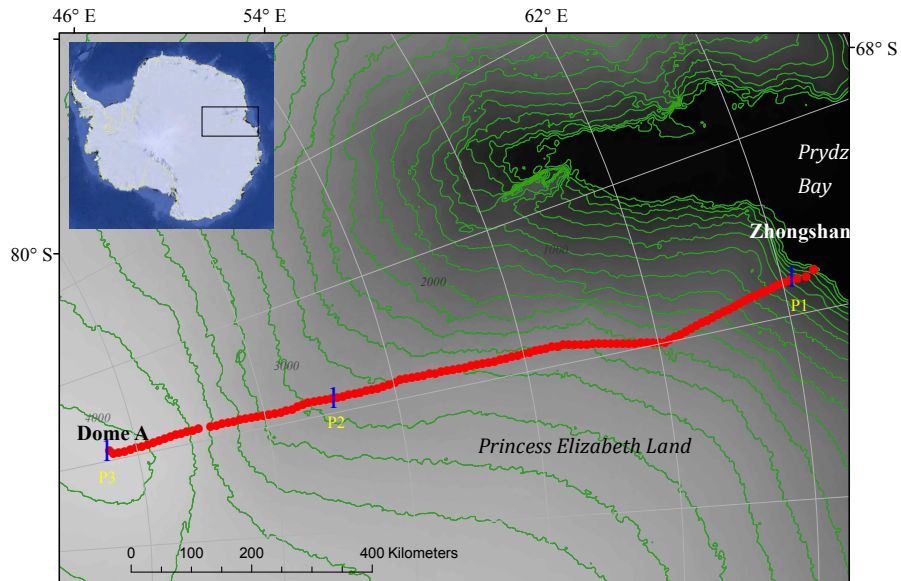
883 \* . Correlation is significant at the 0.05 level (2-tailed).

884

885



886

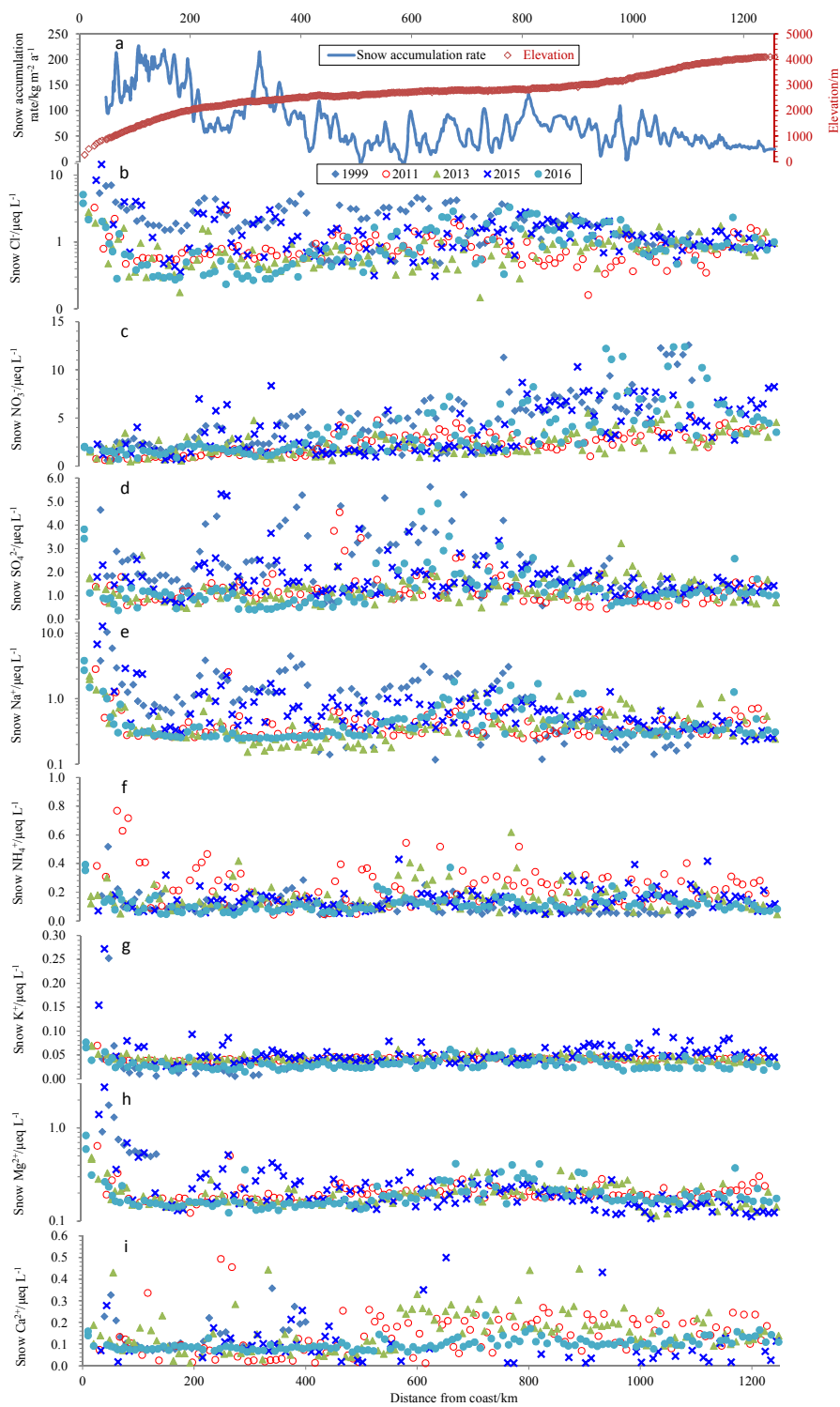


887

888 **Figure 1.** The Chinese inland investigation traverse from the coast (Zhongshan station) to the ice sheet

889 summit, Dome A, East Antarctica. The traverse is generally along the 77.0 °E longitude.

890

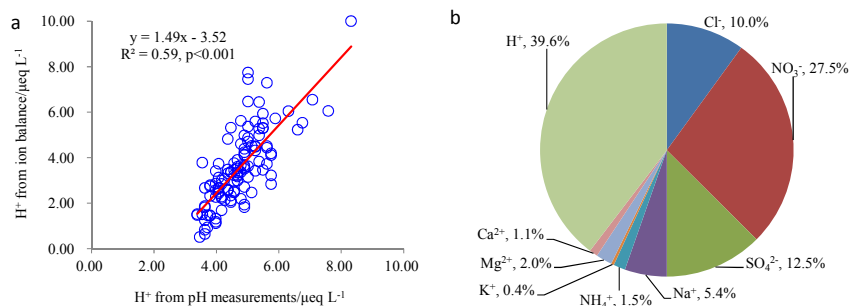




892 **Figure 2.** Annual snow accumulation rate, elevation (a) and ion concentrations in surface snow  
893 collected during five seasons (b-i). Annual snow accumulation rate is obtained from field bamboo stick  
894 measurements, updated to 2016 from Ding et al. (2011). The closed diamond, open circle, closed  
895 triangle, cross and closed circle denote ion concentrations in the years 1999, 2011, 2013, 2015, and  
896 2016, respectively. Note that a base-10 log scale is used for the y-axis of Cl<sup>-</sup> (b), Na<sup>+</sup> (e), and Mg<sup>2+</sup> (h).  
897



898



899

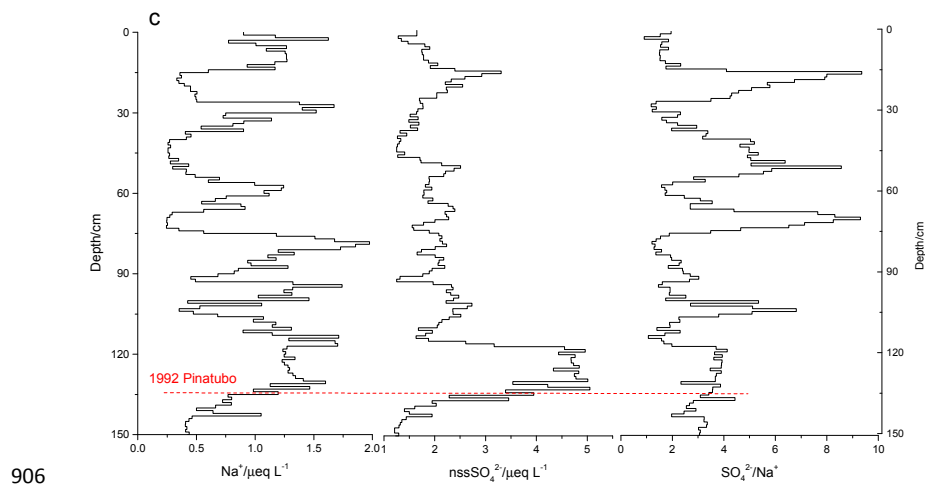
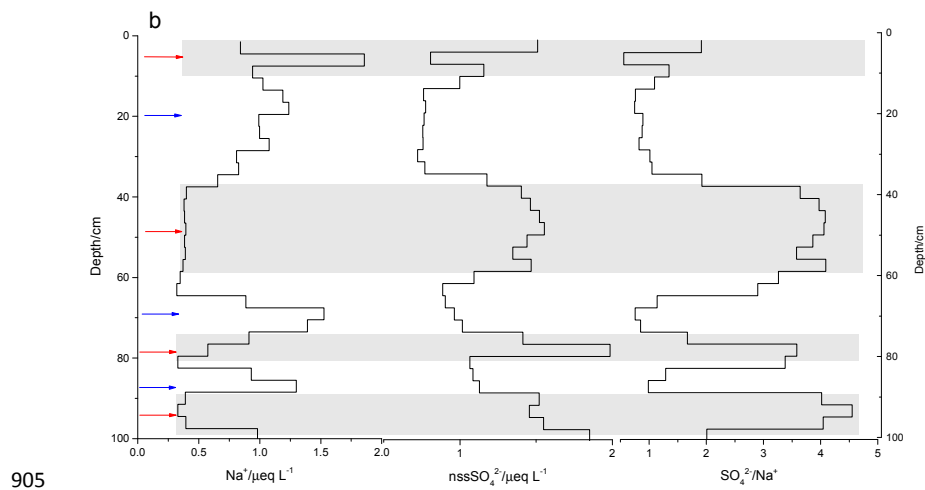
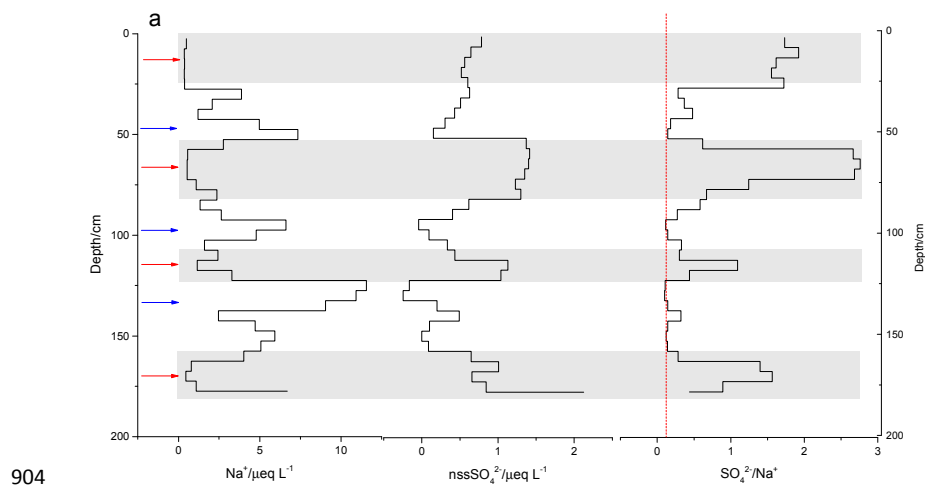
900

901

902

903

**Figure 3.** Major ions in surface snow on the Chinese inland Antarctic traverse. Concentrations of  $H^+$  derived from pH versus those from the ion balance method are shown in panel (a), and contribution percentages of each ion to the total are shown in panel (b), in  $\mu\text{eq L}^{-1}$ .

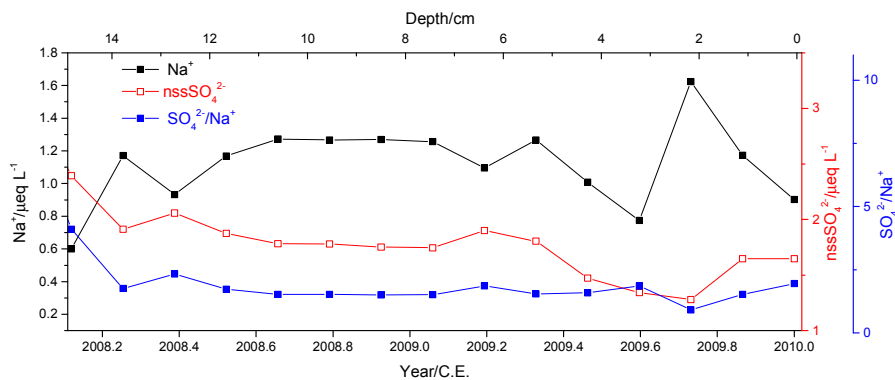




907 **Figure 4.** Profiles of  $\text{SO}_4^{2-}$ ,  $\text{Na}^+$ , and  $\text{SO}_4^{2-}/\text{Na}^+$  ratios in snow pits P1 (a), P2 (b), and P3 (c). Red and  
908 blue arrows in panels (a) and (b) represent the middle of the identified summer and winter seasons,  
909 respectively, and shaded areas denote summer seasons (see text). The red dashed line in panel (a)  
910 represents the ratio of  $\text{SO}_4^{2-}/\text{Na}^+$  in bulk seawater, while the red dashed line in panel (c) signifies the  
911 first snow sample significantly influenced by the Pinatubo eruption. One seasonal cycle generally  
912 represents local  $\text{Na}^+$  minima and  $\text{nssSO}_4^{2-}$  and  $\text{SO}_4^{2-}/\text{Na}^+$  maxima.  
913



914



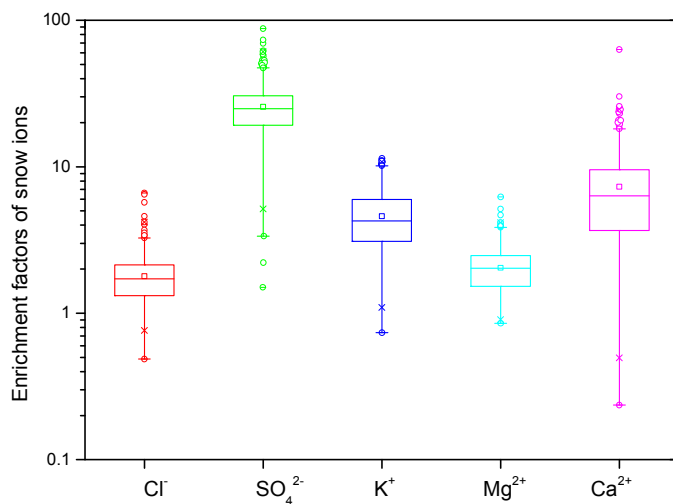
915

916 **Figure 5.** Variations in Na<sup>+</sup>, nssSO<sub>4</sub><sup>2-</sup>, and SO<sub>4</sub><sup>2-</sup>/Na<sup>+</sup> ratio in the snow in the years 2008 and 2009, in  
917 Dome A snow pit (P3).

918



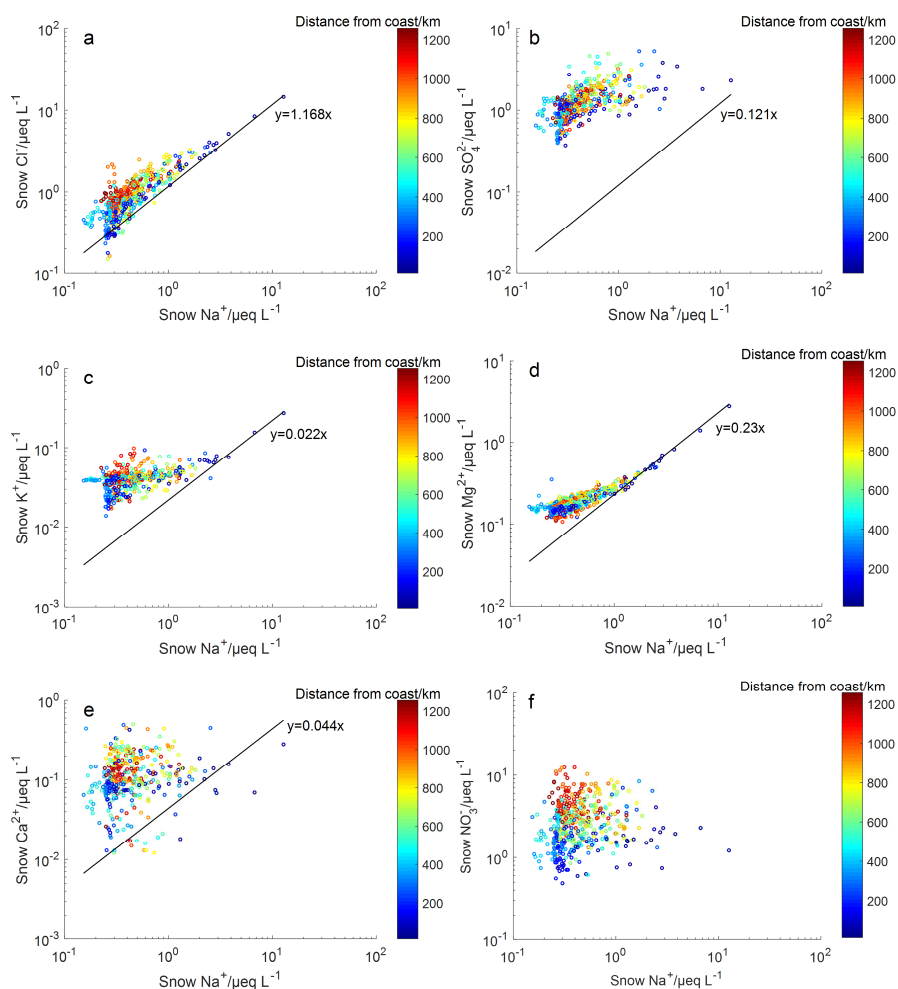
919



920

921 **Figure 6.** Statistics of enrichment factors of ions in surface snow. Box and whisker plots represent  
922 maximum (top end dash symbol for each box), minimum (bottom end dash symbol for each box),  
923 range 1-99 % (top and bottom X symbol for each box), percentiles (5th, 25th, 75th, and 95th), and  
924 median (50th, solid line) and mean (open square near the center of each box). Note that the data outside  
925 the range 5-95 % are shown as open circles.

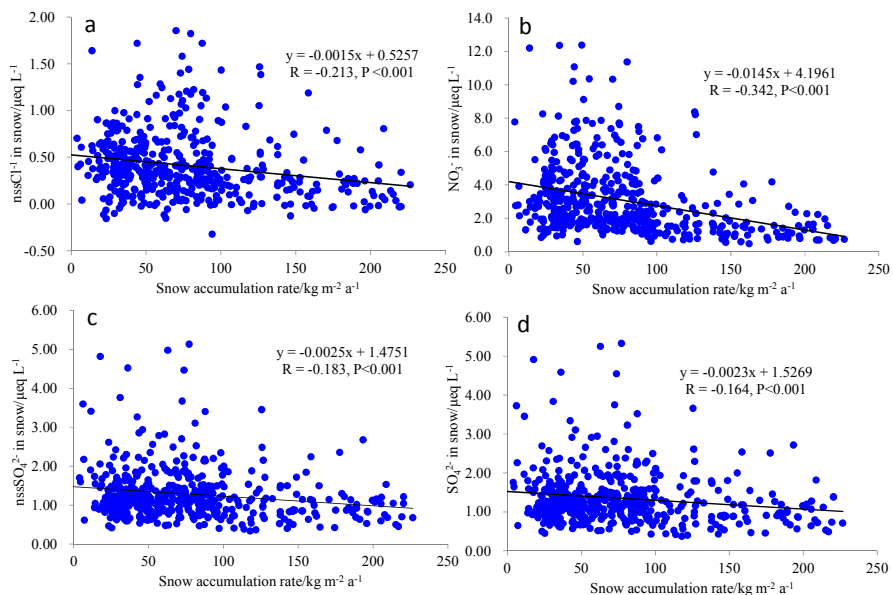
926



927  
928 **Figure 7.** Correlation plots of  $\text{Cl}^-$ ,  $\text{SO}_4^{2-}$ ,  $\text{K}^+$ ,  $\text{Mg}^{2+}$ ,  $\text{Ca}^{2+}$ , and  $\text{NO}_3^-$  versus  $\text{Na}^+$  in surface snow. The  
929 black solid line represents the seawater dilution line, with slopes of typical ions versus  $\text{Na}^+$   
930 concentrations in seawater (in  $\mu\text{eq L}^{-1}$ ). The concentration of  $\text{NO}_3^-$  in seawater is too variable among the seas, and a  
931 representative ratio of  $\text{NO}_3^-/\text{Na}^+$  cannot be presented. Note that a base-10 log scale is used for ion  
932 concentrations.  
933



934



935

936

**Figure 8.** Relationship between chemical ions in surface snow and snow accumulation rate on the traverse.

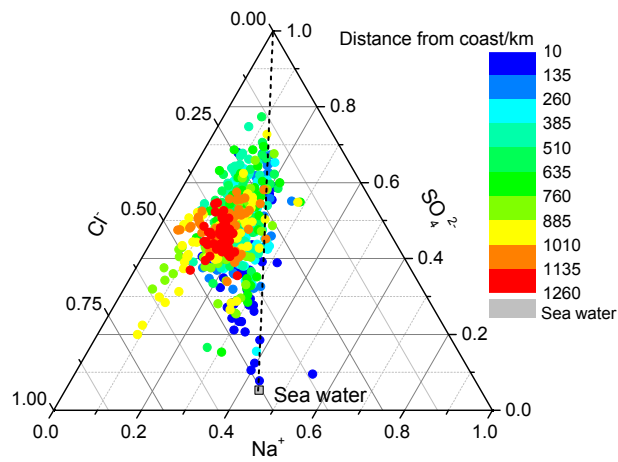
937

938

939



940

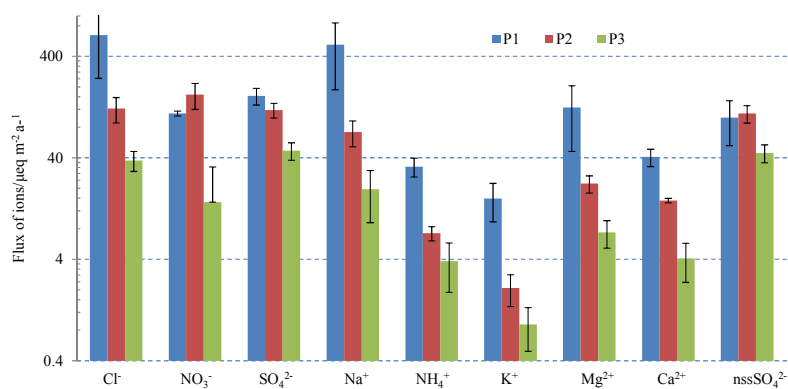


941

942 **Figure 9.** Ternary plot of  $\text{Cl}^-$ ,  $\text{Na}^+$ , and  $\text{SO}_4^{2-}$  in surface snow samples. Bulk seawater composition is  
943 denoted by a grey square. The dashed line extending between the sea salt reference value and the  $\text{SO}_4^{2-}$   
944 summit represents the composition of sea salt with increasing  $\text{SO}_4^{2-}$ .  
945



946



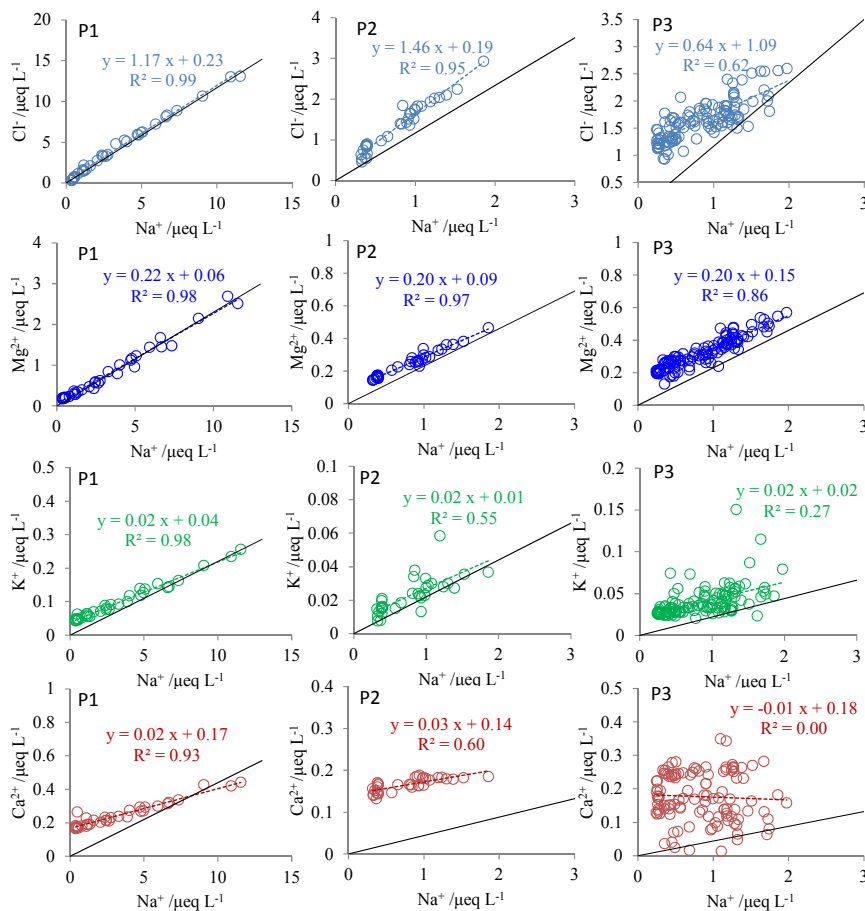
947

948 **Figure 10.** Ion fluxes at the three pits (P1, P2, and P3). The error bars represent one standard deviation  
949 of fluxes in different years. Note that a base-10 log scale is used for the  $y$ -axis.

950



951

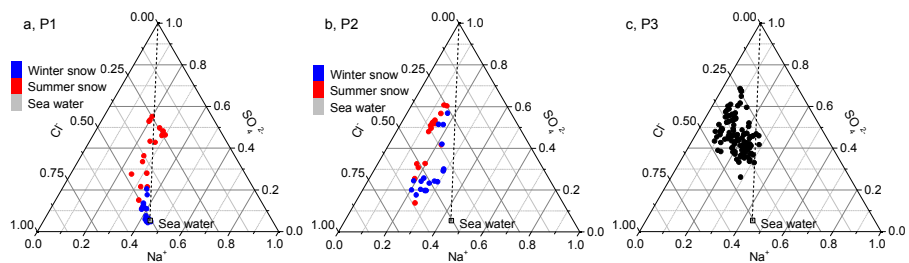


952

953 **Figure 11.** Relationships between Na<sup>+</sup> and Cl<sup>-</sup>, K<sup>+</sup>, Mg<sup>2+</sup>, Ca<sup>2+</sup> in the three snow pits (P1, P2, and P3).  
 954 Also shown are the linear regressions between them (dashed line), with all of the linear correlation  
 955 significant at p<0.001 except Ca<sup>2+</sup>/Na<sup>+</sup> at P3. The black solid line represents seawater dilution line.

956

957



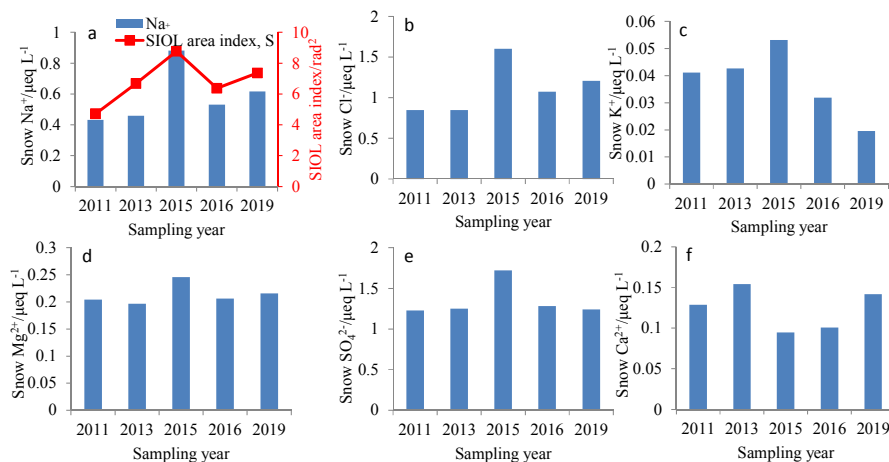
958

959 **Figure 12.** The same as Fig. 7, with blue and red dots in panels (a) and (b) representing winter and  
960 summer snow, respectively.

961



962



963

964 **Figure 13.** Averaged ion concentrations in surface snow collected on the traverse in different years.  
965 The area index of the Southern Indian Ocean low (SIOL), S, is shown in panel (a), calculated following  
966 Wang et al. (2007). The mean sea level pressure from ERA-interim reanalysis during the austral  
967 summers in 2010/2011, 2012/2013, 2014/2015, 2015/2016, and 2018/2019 was used to calculate the  
968 values of S (Figure S3).

969